(Re)Discovering the Seismicity of Antarctica: A New Seismic Catalog for the Southernmost Continent

Andres Felipe Peña Castro^{*1}, Brandon Schmandt¹, Jenny Nakai², Richard C. Aster³, and Julien Chaput⁴

Abstract

We apply a machine learning (ML) earthquake detection technique on over 21 yr of seismic data from on-continent temporary and long-term networks to obtain the most complete catalog of seismicity in Antarctica to date. The new catalog contains 60,006 seismic events within the Antarctic continent for 1 January 2000–1 January 2021, with estimated moment magnitudes ($M_{\rm w}$) between –1.0 and 4.5. Most detected seismicity occurs near Ross Island, large ice shelves, ice streams, ice-covered volcanoes, or in distinct and isolated areas within the continental interior. The event locations and waveform characteristics indicate volcanic, tectonic, and cryospheric sources. The catalog shows that Antarctica is more seismically active than prior catalogs would indicate, examples include new tectonic events in East Antarctica, seismic events near and around the vicinity of David Glacier, and many thousands of events in the Mount Erebus region. This catalog provides a resource for more specific studies using other detection and analysis methods such as template matching or transfer learning to further discriminate source types and investigate diverse seismogenic processes across the continent.

Cite this article as Peña Castro, A. F., B. Schmandt, J. Nakai, R. C. Aster, and J. Chaput (2024). (Re)Discovering the Seismicity of Antarctica: A New Seismic Catalog for the Southernmost Continent, *Seismol. Res. Lett.* **XX**, 1–19, doi: 10.1785/0220240076.

Supplemental Material

Introduction

The apparent aseismicity of the Antarctic continent has long been debated. Multiple studies (Evison, 1967; Sykes, 1978; Johnston, 1987, 1989) have hypothesized that the tectonic earthquakes might be very rare in the interior of Antarctica because the ice sheet suppresses earthquake activity, because low tectonic stress is transmitted to the interior of the Antarctic plate, and/or because the majority of the continent is occupied by old and tectonically inactive Precambrian provinces. Prior to the last two decades, observations and studies of earthquakes in Antarctica were few (Lander, 1959, 1962; Oborina and Sytinskiy, 1978; Adams et al., 1985; Adams and Akoto, 1986; Kanao, 2014) and were often constrained by only a small number of seismic stations, with nearest stations located at distances exceeding 500 km in some cases. Spatially sparse networks greatly increase epicentral uncertainty, prevent accurate depth estimates and compromise the magnitude of completeness of any catalog. Expansion of long-term and temporary seismic instrumentation in Antarctica and elsewhere in the southern hemisphere and the development of new procedures to identify seismic events have increasingly led to recognition that the Antarctic continent is more seismically active than sometimes previously presumed, yet still has a low tectonic seismicity rate compared to other continental interiors of similar size

(Rouland et al., 1992, 2003; Reading, 2002, 2007; Winberry and Anandakrishnan, 2003).

Over the past decades, multiple temporary seismic networks of various scales have been deployed in multiple regions within the Antarctic continent, and their data have been archived in community data centers. Notable deployments include the Transantarctic Mountains Seismic Experiment (TAMSEIS; Pyle et al., 2010), the Transantarctic Mountains Northern Network (TAMNNET; Hansen et al., 2015), the Gamburtsev Antarctic Mountains Seismic Experiment (Hansen et al., 2010), the Polar Earth Observing Network (POLENET; Accardo et al., 2014), the Ross Ice Shelf deployment (RIS/DRIS; Bromirski et al., 2015), and the Antarctic Network of Unattended Broadband Seismometers (Anandakrishnan et al., 2000). Many countries (e.g., United Kingdom, Italy, France,

^{1.} Department of Earth and Planetary Sciences, University of New Mexico, Albuquerque, New Mexico, U.S.A., https://orcid.org/0000-0001-8055-1977 (AFPC); 2. U.S. Geological Survey, Alaska Volcano Observatory, Anchorage, Alaska, U.S.A., https://orcid.org/0000-0002-4559-9796 (JN); 3. Department of Geosciences, Warner College of Natural Resources, Colorado State University, Fort Collins, Colorado, U.S.A., https://orcid.org/0000-0002-0821-4906 (RCA); 4. Department of Earth, Environmental, and Resource Sciences, University of Texas, El Paso, Texas, U.S.A.

^{*}Corresponding author: andresfpenacastro@gmail.com

[©] Seismological Society of America

Korea, Germany, and United States) also maintain scientific research bases that host long-operating seismic stations (including components of the Global Seismographic and GEOSCOPE networks; for more details, see Data and Resources) (e.g., Aster et al., 2004; Park et al., 2014; Schweitzer et al., 2014; Anthony et al., 2015, 2021; Brisbourne et al., 2016; Ringler et al., 2022; Bès de Berc et al., 2023; Leroy et al., 2023).

These networks and stations serve multiple science objectives that include investigating crustal and mantle structure (Hansen et al., 2009; Chaput et al., 2014; Hansen et al., 2014; Shen et al., 2018; Wiens et al., 2023), cryospheric seismic source processes (Martin et al., 2010; Heeszel et al., 2014; Hammer et al., 2015; Winberry et al., 2020; Lucas et al., 2023a; Wiens et al., 2024), estimating ice thickness (Nøst, 2004;Pham and Tkalčić, 2018), characterizing temporal and spatial variations in ambient seismic noise and ocean state (Baker et al., 2019), and studying regional or local seismic events (Winberry and Anandakrishnan, 2003; Lough et al., 2018; Lucas et al., 2021). Figure 1a shows the locations of previously reported seismicity from multiple studies. Examples of seismicity detected include: Lough et al. (2013) detected 27 earthquakes in East Antarctica, Winberry and Anandakrishnan (2003) reported 20 seismic events in the West Antarctic rift system, and Lucas et al. (2021) found 117 seismic events (including 11 inferred earthquakes) in central West Antarctica. Although these individual studies show that some regions in Antarctica are seismically active, there is no long term and uniformly processed seismic catalog available for the Antarctic continent making full use of these varied data sources.

High-quality seismic catalogs are crucial for identifying active fault systems (Liu et al., 2020; Tan et al., 2021), probing earthquake or icequake nucleation, rupture, and triggering processes (Paul Winberry et al., 2013; Peng et al., 2014; Li et al., 2021; DeSalvio and Fan, 2023), or analyzing the rheology and seismogenic processes of faults (Beeler et al., 2013), glacier beds (Hudson et al., 2023), dynamics of glaciers (Aster and Winberry, 2017), and ice shelves (Aster et al., 2021; Huang et al., 2022). In this study, we present a seismic catalog for the Antarctic continent built using a deep learning (DL) phase picker (Mousavi et al., 2020) and utilizing ~21 yr of openly accessible seismic data. The resulting catalog contains 60,006 events representing a wide variety of source processes. In the next sections, we describe the methodology to build the catalog, present preliminary observations and interpretations, and discuss the limitations and possible future applications of the catalog and its methodology.

Building the Seismic Event Catalog

We used 21 yr of continuous community data from stations located south of latitude -60° between 1 January 2000 and 1 January 2021. All data are openly accessible from the Data Management Center of the EarthScope Consortium supported by the U.S. National Science Foundation's award for Seismological Facilities for the Advancement of Geoscience.

Figure 1b shows seismograph locations used in the study. These include both permanent and temporary stations and networks. We downloaded broadband, high-broadband, short-period, and extremely short-period channels.

We used Earthquake Transformer (EQTransformer, Mousavi et al., 2020), a DL model, for detecting earthquakes and estimating P-wave and S-wave phase arrival times. We used the implementation of the EQTransformer phase picker that is integrated into SeisBench (Münchmeyer et al., 2022; Woollam et al., 2022), an open-source Python toolbox for ML in seismology. SeisBench provides the option to train EQTransformer with different data sets, but here we use the default STanford EArthquake Data set (STEAD) to train the network (Mousavi et al., 2019). STEAD is a large-scale global data set of labeled earthquake and noise signals. STEAD has data from earthquakes at epicentral distances ranging from 0 to 350 km and magnitudes ranging from -0.8 to 8, but with the majority of these events located at distances <110 km and magnitudes less than 2.5. We applied EQTransformer to the 21 yr of piecewise continuous data and retained picks above a probability threshold of 0.01 for earthquake detection, P wavepick, and S wavepick. We chose this low threshold given that the spatially sparse seismic data from Antarctica were acquired under unique and seasonally variable noise and/or station conditions (Anthony et al., 2015) compared to other regions on Earth. These characteristics include (1) the extremely high winds on the Transantarctic Mountains (Mayewski et al., 2009) and Antarctic Peninsula, (2) extremely cold temperatures, and (3) stations deployed in ice boreholes, shallow snow vaults, or other atypical situations. Assigning a low probability threshold for event declaration and phase picks allows for the consideration of a large number of potential phase arrivals, which we cull during subsequent phase association and hypocenter estimation workflow steps.

P and S phase picks generated by EQTransformer were associated into events or discarded using the rapid earthquake association and location (REAL) package (Zhang et al., 2019). REAL is a grid-search-based method that requires a 1D velocity model to associate the picks, for which we used the global velocity model ak135 (Kennett et al., 1995). The grid encompasses search ranges with station-event distances up to 1.6° (178 km), a geographic grid size of 0.05° (5.6 km), and event depths ranging from 0 to 60 km with a grid size of 10 km. We required a minimum of six phase arrivals (P or S), in which at least two stations recorded both the *P* and *S* arrivals. To refine location quality and discard poorly constrained events, we applied Non-Linear Location (NLLoc) software (Lomax et al., 2000, 2009). For consistency, we use the same velocity model (ak135) in NonLinLoc in a global coordinate system, and limiting the maximum depth search to 100 km in the case of possible events deeper than 60 km. The NonLinLoc methodology applies efficient global sampling algorithms to obtain an estimate of the 3D posterior probability density function (PPDF)

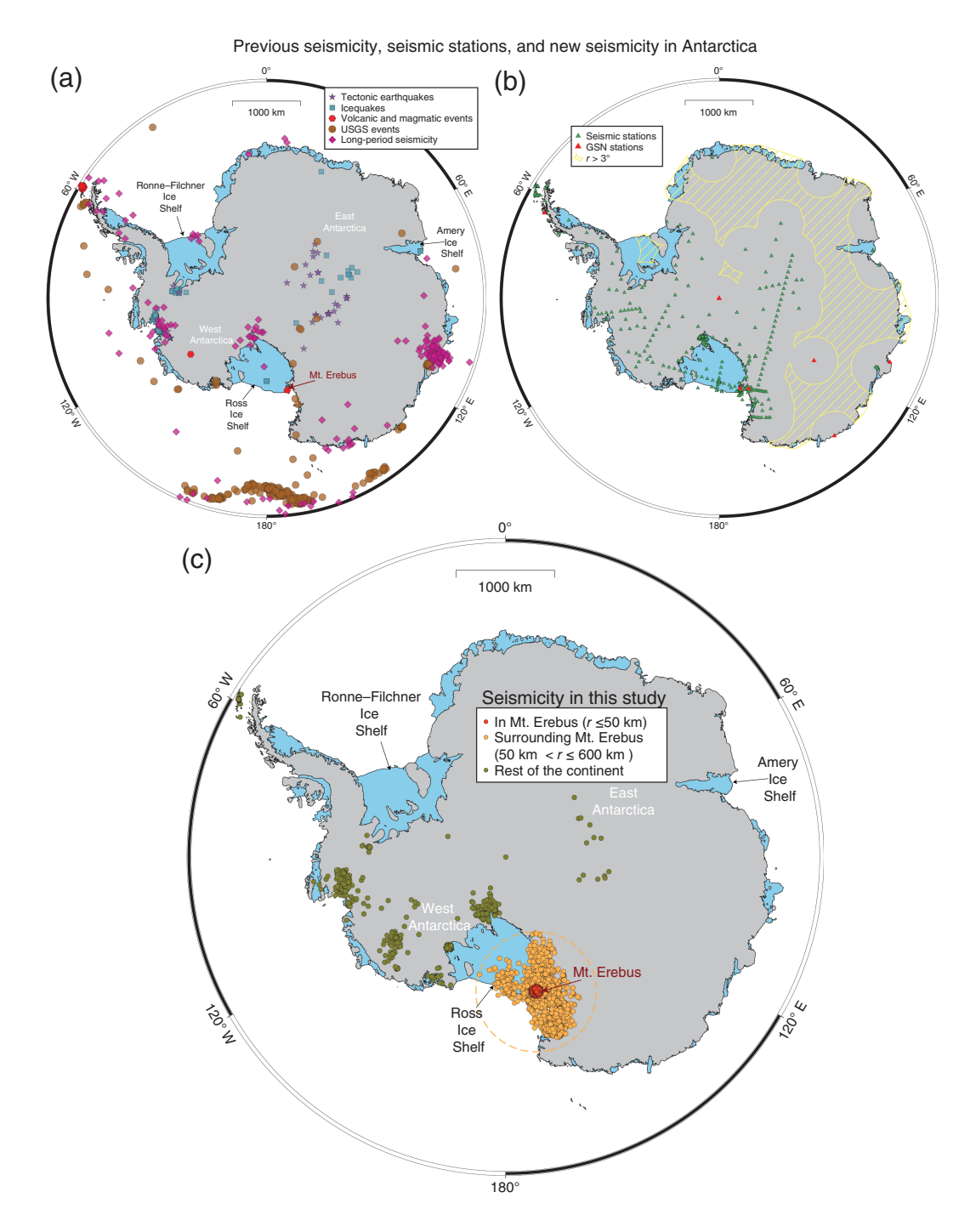


Figure 1. (a) Seismicity as previously reported by various studies in the Antarctic continent. Dark stars represent tectonic seismicity reported by Lough *et al.* (2018) and Lucas *et al.* (2021). Dark blue squares represent icequakes reported by Heeszel *et al.* (2014), Lough *et al.* (2015), Lombardi *et al.* (2019), Hudson *et al.* (2021), Kufner *et al.* (2021), Lucas *et al.* (2021), Winter *et al.* (2021), and Huang *et al.* (2022). Red hexagons represent seismicity associated to volcanic activity reported by Rowe *et al.* (2000), Lough *et al.* (2013), and Olivet *et al.* (2021). Brown circles represent all seismic events reported by the U.S. Geological Survey (USGS) between 1 January 2000 and 1 January 2021 (see Data and Resources). Purple diamonds represent long-period (≈25–100 s) glacial seismicity detected by Nettles and Ekström (2010), Chen *et al.* (2011), and Poli (2023). (b) Distribution of seismic stations (green

triangles) deployed in Antarctica between 1 January 2000 and 1 January 2021. Stations from the Global Seismograph Network (GSN) are shown as red triangles. The yellow stipple polygons represent regions that are farther away than 3° from any recording station. (c) Detected seismicity reported in this study. The Mount Erebus (red circles) and Ross Island region has the greatest number of detected events in the catalog (47,961). The regions surrounding Mount Erebus, that is, between 50 and 600 km (orange dashed circle) concentric radius circles, also include a large number of detected events (10,619). The remaining regions of the continent have 1426 seismic event detections. Seismicity is broadly located near Ross Island, proximal to large glaciers, and in isolated areas within the continental interior. The color version of this figure is available only in the electronic edition.

for the absolute hypocenter location. The PPDF provides a probabilistic description of the hypocenter parameters and associated uncertainty estimates. Within NLLoc, we apply an equal differential time likelihood function (Font et al., 2004; Lomax, 2005, 2008), which is robust in the presence of outlier data caused by large phase identification errors and large residuals between measured and predicted travel times. We noticed that some of the picks have large residuals (or picks are assigned low weights) and visual inspection of waveforms confirmed that many of these were false picks or incorrect associations (e.g., Fig. S1, available in the supplemental material to this article). We removed those large residual or low-weighted picks so they did not contribute to minimum pick thresholds and relocated such events. At this step, we removed ≈1,200,000 events and retained ≈550,000 events. We then applied quality control criteria to retain the events with horizontal and vertical errors ≤50 km and azimuthal station coverage gaps ≤270°. For the abundant seismicity near Mount Erebus volcano and McMurdo Sound (radius ≤50 km), we applied a higher quality control of 25 km since this region has hosted more stable and denser seismic networks compared to the rest of the continent.

Magnitudes for all the events with acceptable locations were computed using spectral inversion of the seismograms windowed around their S-wave arrivals. We used the SourceSpec package (Satriano, 2022) to compute moment magnitudes, with a window length of 5 s, starting 1 s before the S-wave arrival time. We choose a fixed window length given that the majority events in our catalog must have magnitudes < 4.5 and maximum source-station distances of ~350 km (based on the training data set of STEAD). We recognize that the 5 s might be a long window for small events with short source-station distance because that window will include some coda; therefore, the magnitude reported should be considered an upper limit in those cases. For each seismogram, the noise spectrum was calculated in an equal length window starting 6 s before the *P* arrival time. We required a minimum signal-to-noise ratio (SNR) of 1.5 for contributions to the magnitude estimation and report the mean value of all the magnitude estimates for each event. Figure S2 shows an example of moment magnitude estimation for a typical event and the model fit to the observed spectra. All events in the catalog have an assigned magnitude. We acknowledge that our catalog is incomplete and that more seismic events are thus present in Antarctica within our magnitude range than what we reported in this study because our multiple requirements (azimuthal gap, location uncertainty, and SNR) reduced the number of events but increased the catalog quality and uniformity.

Results

We located a total of 60,006 events with the quality control criteria described in the previous section. Figure 1c shows the location of all the events. For an initial characterization of the catalog, we divide the seismicity into three regions:

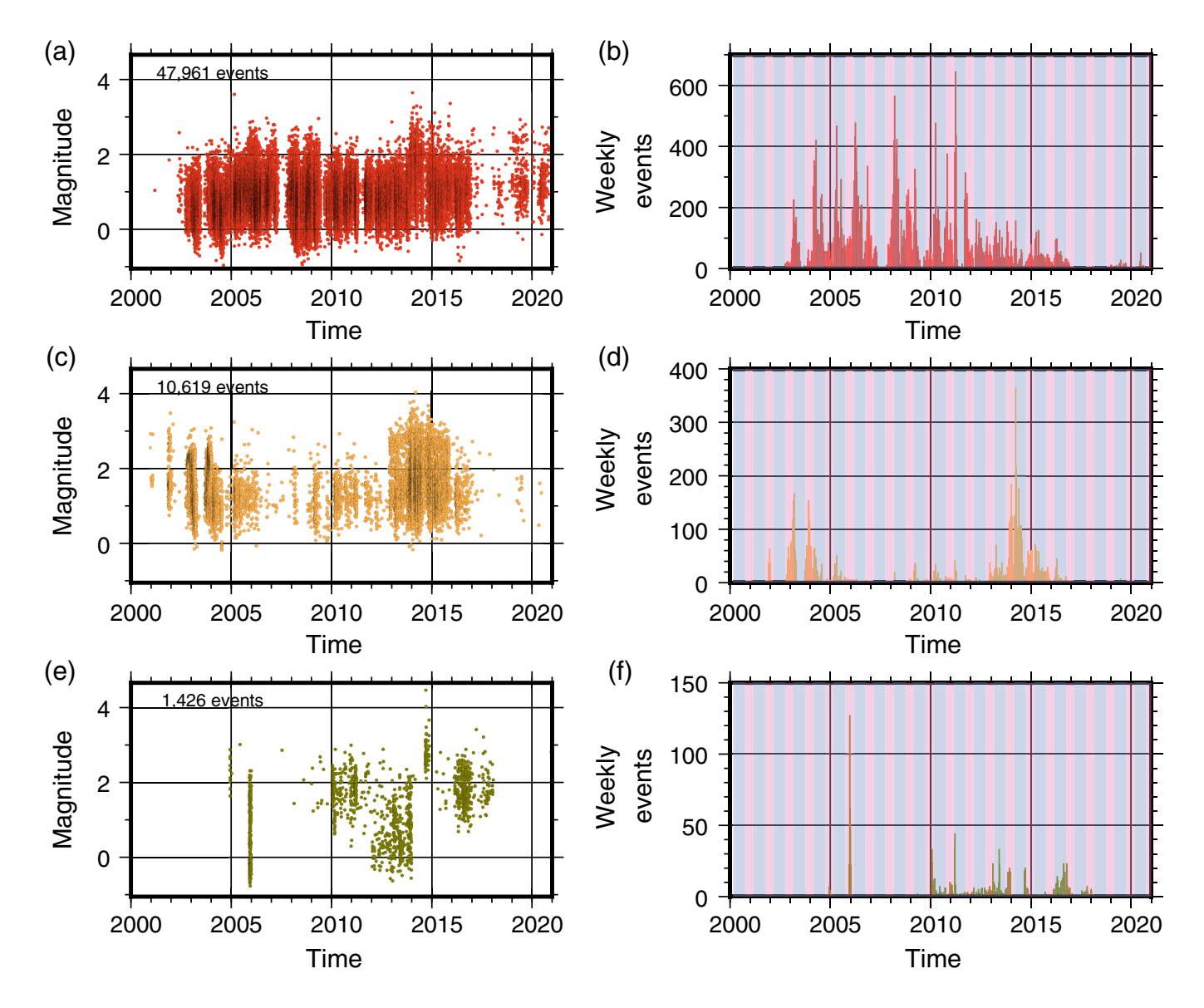
on and near Mount Erebus, the region surrounding Mount Erebus and Ross Island, and the rest of the continent. We define seismicity on and near Mount Erebus as events enclosed by a circle with a radius of 50 km centered on the summit. We will refer to the seismicity surrounding Mount Erebus or Ross Island as the events within an annulus enclosed between the two concentric circles, one with an external radius of 600 km and the other with an internal radius of 50 km centered at the summit. We will refer to the seismicity elsewhere as encompassing the rest of the continent. We choose this division because there is a notably greater density of located events at Mount Erebus volcano and its surroundings.

Most detected seismicity is concentrated in the immediate region within 50 km of Mount Erebus (red circles in Fig. 1c), followed by the surroundings of Mount Erebus (orange circles in Fig. 1c), and the rest of the continent (dark yellow circles in Fig. 1c). We detected \approx 48,000 (80%) in the immediate vicinity of the volcano with magnitudes ranging from -1.0 up to 3.6 (Fig. 2a,b). In the annular region between 50 and 600 km centered on Mount Erebus, we found \approx 10,600 events (17.7%) with magnitudes ranging between -0.2 and 4.1 (Fig. 2c,d). For the rest of the continent, we found \approx 1400 events with magnitudes varying between -0.7 and 4.5 (Fig. 2e,f).

The prolific detection of seismic events in the Erebus region reflects both the relatively high level of seismic activity associated with the active Mount Erebus volcano, as well as the relatively long-term history of seismic data collection there for monitoring and research (Sims *et al.*, 2021). Figure 2a,b shows that an increase in detected seismicity at Mount Erebus starting in 2002 that correlates with the installation of multiple new technology permanent seismic stations on the flanks of Mount Erebus volcano during the 2002–2003 and 2003–2004 field seasons (Aster *et al.*, 2004). Some gaps in detected seismicity between 2002 and 2016 are attributable to austral winter power (blue vertical shades in Fig. 2b) or telemetry issues and associated station downtime (Knox *et al.*, 2018).

Detected seismicity surrounding Ross Island is less temporally continuous than at Mount Erebus (Fig. 2c,d), reflecting when temporary regional networks were operating. These notably include (1) TAMSEIS (Lawrence et al., 2006a,b; Watson et al., 2006; Pyle et al., 2010), deployed between the Ross Sea and the Vostok Highlands (see Fig. S3 for other relevant geographic points in Antarctica) and consisting of 42 temporary broadband stations deployed from November 2000 to December 2003, (2) TAMNNET (Hansen et al., 2015), which operated from late 2012 through late 2015 with 15 stations, and (3) the RIS/DRIS network, which consists of 34 stations deployed on and adjacent to the Ross Ice Shelf (Bromirski et al., 2015; Baker et al., 2019) between late 2014 and early 2017, among other networks.

The seismicity in the rest of the continent in our catalog is more sporadic (Fig. 2e,f) in comparison with the region surrounding Mount Erebus because most detection thresholds



are dictated by the presence of temporary networks. For example, the vertical streak at the end of 2005 shown in Figure 2e,f corresponds to the events detected in the Siple Coast by a temporary array of 13 stations (network code ZD) deployed from mid-December to mid-January, whereas the seismicity that occurred between 2015 and 2017 reflects events detected by temporary instrument deployments within the United Kingdom Antarctic Network and the Polar Earth Observing Network (POLENET/ANET), both located in West Antarctica. Figure 2b,d,f shows the weekly number of events versus time displaying the higher number of events during the austral summer (pink vertical shade) and more sporadic seismicity that follows the presence of temporary networks.

We detected seismic events in multiple regions of Antarctica, including East Antarctica, Mount Erebus, Ross Ice Shelf, Marie Byrd Land, Victoria Land, Ellsworth Land, Queen Maud Mountains, the Siple Coast, and near outlet glaciers (Thwaites Glacier, Pine Island Glacier, or David Glacier). The large variety of regions where seismicity is present suggests that

Figure 2. Event magnitudes versus time and weekly events versus time for (a,b) Mount Erebus, (c,d) regions surrounding Mount Erebus, and (e,f) rest of the continent. Number on the top right of (a,c,e) represents the number of events in each plot (Fig. 1c). Blue and pink shaded regions in (b,d,f) represent winter and summer seasons, respectively. Earthquake detections are more continuous in time at Mount Erebus and surroundings because of the presence of a relatively long-running (decades) and continuously operating seismic network on Mount Erebus volcano. In contrast, detections across the rest of the continent are more sporadic because they largely depend on temporary seismic station deployments. The color version of this figure is available only in the electronic edition.

the catalog contains both tectonic and cryospheric events, as well as in some cases magmatic and volcanic processes.

Preliminary Observations: Icequakes

Many studies (e.g., Smith, 2006; Zoet et al., 2012; Paul Winberry et al., 2013; Smith et al., 2015; Podolskiy and Walter, 2016; Aster and Winberry, 2017; Kufner et al., 2021) have shown that the

cryosphere generates a wide variety of seismic signals, broadly referred to as icequakes. Icequakes are the manifestations of varied cryosphere processes and adjoining (solid Earth or water) media including: (1) crevasse formation (Walter et al., 2008, 2009), (2) stick-slip motion at the ice-bedrock interface (Smith, 2006; Allstadt and Malone, 2014; Smith et al., 2015), (3) iceberg calving (Richardson et al., 2012), (4) snow and firn cracking (Lough et al., 2015), or (5) glacier rumbling (Rial et al., 2009), among many other processes. Icequakes span large variety of magnitudes ($M \approx -3$ to 7), in which the maximum magnitude reported corresponds to long-duration (~25 min) stick-slip motion of a large ice stream in West Antarctica (Wiens et al., 2008), and frequency ranges (10⁻³ to 10² Hz). Moreover, icequake activity has been widely observed across Earth's cryosphere, including: (1) the Columbia and Bering Glaciers in Alaska (Qamar, 1988; O'Neel et al., 2007; Richardson et al., 2012), (2) the Greenland ice sheet and its outlet glaciers (Ekstrom et al., 2003; Röösli et al., 2014), (3) snow-clad volcanoes such as Llaima, Chile (Lamb et al., 2020), and Mount Rainier (United States) (Allstadt and Malone, 2014), (4) glaciers in the European alps (Gräff and Walter, 2021; Gräff et al., 2021), and (5) interior and near-coastal locations across Antarctica (Winberry et al., 2009; Nettles and Ekström, 2010; Lough et al., 2015; Hudson et al., 2021; Kufner et al., 2021; Huang et al., 2022; Poli, 2023).

Previous cryoseismology studies in Antarctica (e.g., Chaput et al., 2015; Chen et al., 2019; Olinger et al., 2019; Kufner et al., 2021; Li et al., 2021; Lucas et al., 2021; Huang et al., 2022; Wiens et al., 2024) have reported activity at the edges and within ice shelves, ice streams (channels of fast flowing ice with ice sheets, Bentley, 1987), near outlet glaciers, or at Mount Erebus. Figure 1a shows the location of reported icequakes (dark blue squares) by Heeszel et al. (2014), Lough et al. (2015), Lucas et al. (2021), Hudson et al. (2021), and Huang et al. (2022). Many events in our seismic catalog are located in similar settings (Fig. 1c). Figure S4 shows the locations of selected ice shelves, outlet glaciers, and ice streams on a continental-scale ice velocity map (Rignot et al., 2017). Event locations overlap with the Ross Ice Shelf, Sulzberger Ice Shelf, Thwaites Ice Shelf, Abbot Ice Shelf, Cosgrove Ice Shelf, MacAyeal Ice Stream (Ice Stream E), the Rutford Ice Stream, and David Glacier.

Cryoseismicity signals are highly variable including: harmonic tremors (MacAyeal *et al.*, 2008; Martin *et al.*, 2010; Paul Winberry *et al.*, 2013), long-period (10–50 s) events (Winberry *et al.*, 2020), short-duration events with distinct *P*- and *S*-wave arrivals (Smith *et al.*, 2015; Minowa *et al.*, 2019), and dispersed Rayleigh wavetrains with weak or absent body waves (Lough *et al.*, 2015; Aster *et al.*, 2021), among others. Figure S5 shows the waveforms for some of these inferred icequakes. We inspect the waveforms of some of the events in our catalog to confirm whether the events have waveform characteristics similar to the types of icequakes shown in Figure S5. Figure 3a shows the location of station S020, located at the MacAyeal Ice Stream (also

known as Ice Stream E) on the Siple Coast. Figure 3a shows ice velocity (Rignot et al., 2017) for this region of Siple Coast and the Ross Ice Shelf, which indicates high ice velocities (>400 m/yr) near the station S020 and near the detected seismicity. Figure 3b shows vertical waveforms from the station S020 for four events detected near the station (≤50 m). The waveforms indicate short-duration events with impulsive Pand S-wave arrivals on the vertical component but no readily visible surface waves (Fig. 3b), which is similar to basal icequakes observed in other regions (Smith et al., 2015; Minowa et al., 2019; Gräff and Walter, 2021; Gräff et al., 2021; Kufner et al., 2021). In addition, the time difference between S- and P-wave arrivals are usually shorter than 0.5 s, which indicates that the events are generated by a shallow source. These icequakes demonstrate that our catalog development workflow detects processes similar to shear rupture on a surface such as stick-slip motion at the ice-bed interface (Smith, 2006; Hudson et al., 2020). Our catalog did not detect tremorlike waveforms from processes such as iceberg collisions (MacAyeal et al., 2008; Martin et al., 2010) and/or fluid-flow-induced vibrations (Muller et al., 2005). This is a consequence of the detection method, which uses an ML phase picker (EQTransformer) with a training data set (STEAD) of local tectonic events. Other ML detection methods (Barkaoui et al., 2021; Sawi et al., 2022) or training data sets (such as tremors or glacial earthquakes) could help detect other types of cryospheric events besides those similar to tectonic events reported here. Traditionally, earthquakes have been explained as rupturing asperities (Lay and Kanamori, 1981) (high frictional patches) that fail at velocities near to (and sometimes exceeding) the medium shear wavespeed. Many icequakes in our seismic catalog, being regionally observed, are probably the result of basal "asperities" at outlet glaciers or ice streams, as has been proposed by Alley (1993), Danesi et al. (2007), and Sergienko and Hulbe (2011). These event detections using a method trained on tectonic seismicity highlight how analogous stick-slip failure and associated seismic signals can be in cryospheric settings (Barcheck et al., 2021).

Repeating earthquakes (events with nearly the same source location and mechanism) have been notably observed at the base of David Glacier, a large outlet glacier in Victoria Land (Danesi et al., 2007; Zoet et al., 2012). Figure 4a shows the location of David Glacier and nearby events in our seismic catalog. We verified that the seismic catalog contains events with waveform similarity. However, other events with low similarity are also detected and located in this vicinity. The nonsimilar events suggest that other source regions and processes are active in addition to the previously noted repeating source asperity (Zoet et al., 2012).

Preliminary Observations: Tectonic Events

Earlier studies of tectonic earthquakes in the Antarctic continent generally note infrequent $M_{\rm w}$ \geq 4–5 events observed by

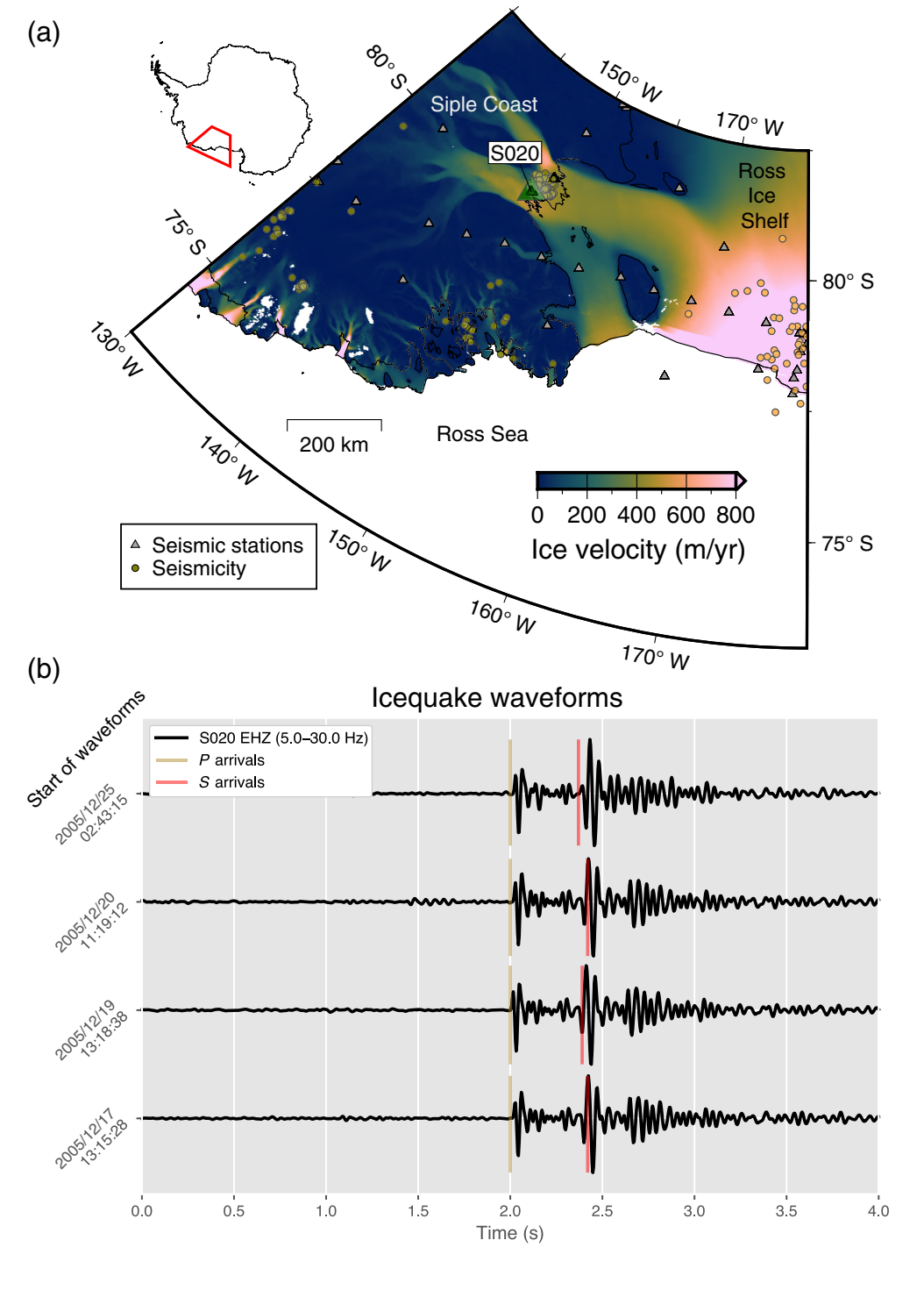


Figure 3. (a) Siple Coast, Ross Sea, and part of the Ross Ice Shelf showing seismic stations (triangles) and seismicity (circles). The background colors indicate annual ice velocity (m/yr) (Rignot *et al.*, 2017). The inset on top left shows the location of the main map with respect to Antarctica. Events are located both on the ice shelf and near major glaciers and ice streams. (b) Vertical waveforms of four highly similar seismic events recorded at station S020, located at Ice Stream E (also known as MacAyeal Ice Stream). Waveforms were filtered between 5 and 30 Hz to highlight the arrivals. Yellow and red vertical lines mark the estimated P and S arrivals (from EQTransformer), respectively. Vertical axis labels show the start of each waveform in Coordinated Universal Time, and horizontal axis time is with respect to the start of the plot. The event locations and short $t_S - t_P < 0.5$ s indicate that these events are cryospheric, that is, icequakes. The color version of this figure is available only in the electronic edition.

temporary arrays that tranenhanced siently regional detection sensitivity (Adams et al., 1985; Adams and Akoto, 1986; Bannister and Kennett, 2002; Winberry and Anandakrishnan, 2003; Lough et al., 2018; Lucas et al., 2021). Early observations of tectonic events come from: (1) Adams (1969) reported 27 events in Victoria Land and interpreted that three could not be attributed to ice movements based on their locations, and (2) Adams and Akoto (1986) reported four events in the continental interior with magnitudes between 4.5 and 5.0. More recently, Bannister and Kennett (2002) reported 84 events with magnitudes less than 3.5 in the Transantarctic Mountains; the physical mechanism of such events is not conclusive given that they are located close to both David fault (Salvini Storti, 1999) and to David Glacier lineament (Bannister and Kennett, 2002). Winberry and Anandakrishnan (2003) analyzed 20 earthquakes that occurred in West Antarctica and may be driven by tectonic activity or magmatic processes. Lucas et al. (2021) identified eleven earthquakes in central West Antarctica (near the Ellsworth Mountains, Mount Takahe, and in the Thwaites Glacier region) based on depth estimates and waveform characteristics. Lough et al. (2018) found 27 intraplate tectonic earthquakes in the interior of East Antarctica.

We detect seismic events in the above regions and estimated similar crustal depths (5 km \leq z \leq 35 km) that are comparable to intraplate earthquakes from other continents

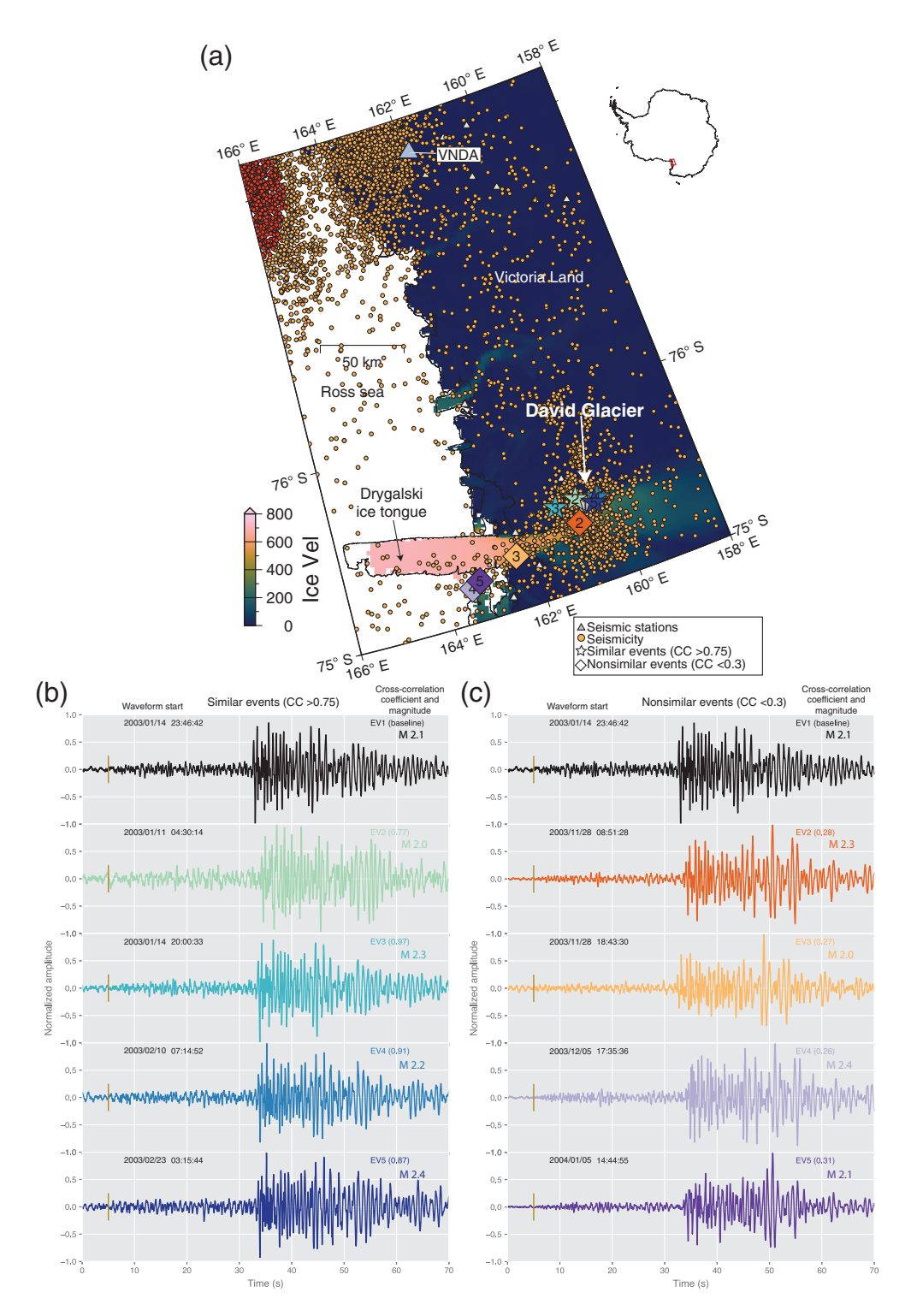
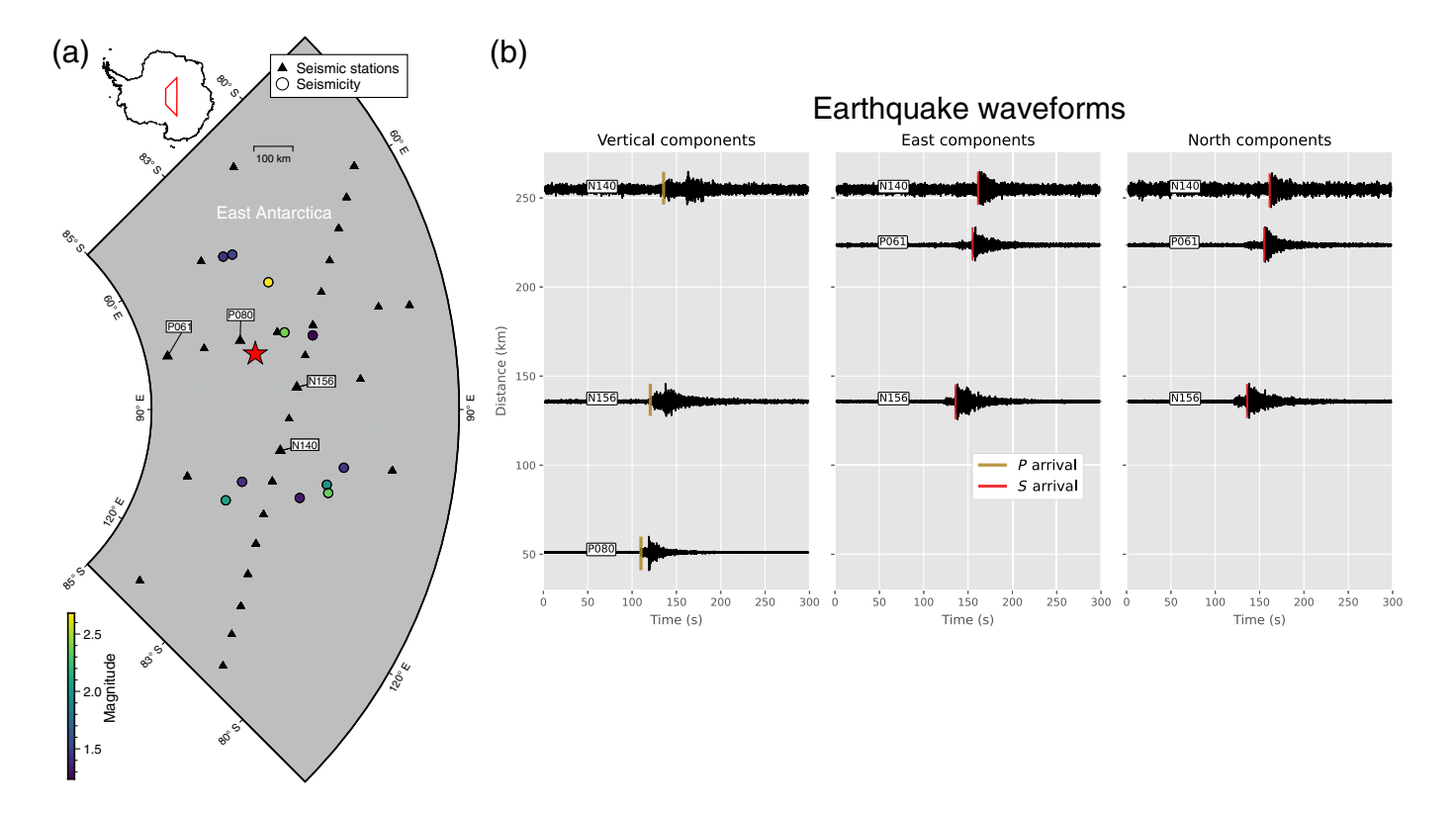


Figure 4. (a) Victoria Land, David Glacier, and Drygalski ice tongue showing seismic stations (triangles) and seismicity (circles). The coast, glacier, and ice tongue are color coded with annual ice velocity (m/yr) (Rignot *et al.*, 2017). The inset on the top right shows the location of the main map with respect to Antarctica. The stars and diamonds represent the locations of selected events with high similarity (cross correlation, CC >0.75) and low similarity (CC <0.3), respectively. (b) Vertical waveforms from station VNDA for five similar events highlighted with colored stars in panel (a). Event 1 (gray star in panel a) was used as a baseline to compute CC. Yellow vertical lines at around 5 s indicate the *P*-wave arrivals. The cross correlation and magnitude for each event is shown on the top right for each waveform, and start times are shown on the top left of each waveform. (c) Same as in panel (b), but waveforms belong to the five nonsimilar events highlighted with colored diamonds in panel (a). The color version of this figure is available only in the electronic edition.

(Talwani, 2014), which suggests that some events in our catalog are related to fault slip. As an example, we show events in the interior of East Antarctica (Fig. 5a), where we detect 12 events with magnitudes ranging between 1.2 and 2.7. Figure 5b shows the waveforms and the respective P- and S-wave arrivals for an event (red star in Fig. 5a) with an $M_{\rm w}$ 1.4.

Preliminary Observations: Volcanic and Magmatic Events

Volcanic and/or magmatic seismicity has been reported at multiple regions in Antarctica: (1) the Executive Committee Range (ECR) (Panter et al., 1994; Lough et al., 2013; Wimez and Frank, 2022), (2) the South Shetland Islands (Olivet et al., 2021; Cesca et al., 2022; Poli et al., 2022), (3) Mount Erebus (Kaminuma et al., 1985; Aster et al., 2003; Dibble et al., 2008), and (4) Mount Melbourne (Gambino and Privitera, 1994, 1996). We detected events in the same regions (Figs. 1c, 5a, and 6a) and near other volcanoes that are less studied (Van Wyk de Vries et al., 2018; Wilch et al., 2021). Figure 6a shows the seismicity detected in the ECR where swarms deep long-period (DLP) magmatic seismicity have been previously identified (Lough et al., 2013). We detected 274 events with an average depth $\bar{z} = 28$ km similar to that reported in Lough et al. (2013) between 25 and 40 km. Figure 6b shows waveforms with *P*- and *S*-wave arrivals for an event located (red star in Fig. 6a) at a depth of 32 km with an $M_{\rm w}$ 1.7. In addition, we confirmed that the events have a

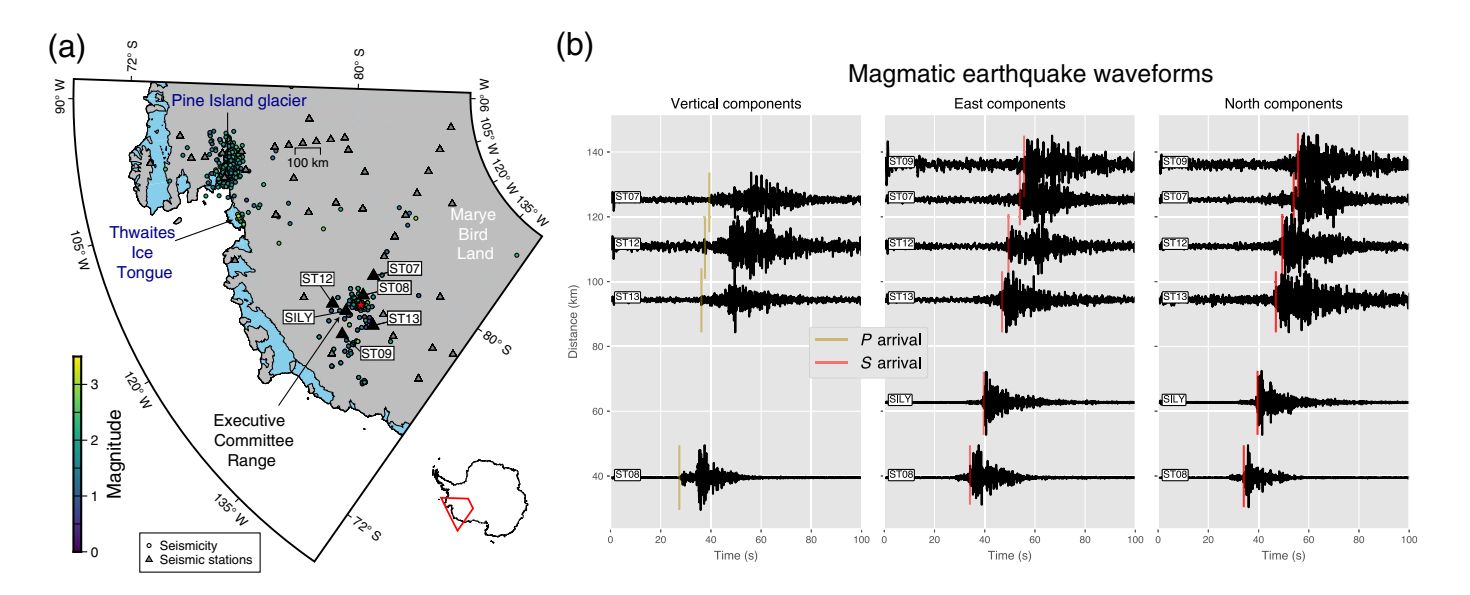


maximum spectral amplitude at $\approx 1-3$ Hz (Fig. S6), similar to the frequency content of previously reported DLP seismicity swarms (Lough *et al.*, 2013).

The region with the greatest concentration of seismicity in the catalog is the persistently active Mount Erebus volcano on Ross Island, for which our catalog contains >45,000 events. Figure 7a shows a source location density map near Mount Erebus. Epicenter estimates are concentrated at and are north to northwest of the summit. Previously reported seismicity types at Mount Erebus volcano includes: very-long-period (VLP; 8-20 s) events associated with lava lake explosions (Rowe et al., 2000; Aster et al., 2003, 2008; Gerst et al., 2013), isolated instances of interpreted volcanic and iceberg tremor (Kaminuma et al., 1985; Rowe et al., 2000; MacAyeal et al., 2008), icequakes on the flanks of the volcano (Chaput et al., 2015; Knox et al., 2018; Li et al., 2021), and occasional noneruptive events, which may be glaciogenic, phreatomagmatic, or volcanotectonic (Kaminuma et al., 1985, 1986). We do not expect to detect all these events unless they are accompanied by impulsive *P* and *S* arrivals. In addition, the numbers of events studied previously is considerably smaller than found in our catalog. For example, Knox et al. (2018) reported 2974 infrasound-corroborated VLP eruptions between 2003 and 2011, Li et al. (2021) detected 7603 icequake events around the origin time of large teleseismic events ($M_w > 7$) between 2000 and 2017 to investigate teleseismic dynamic triggering. A new observation from our seismic catalog at Mount Erebus is that multiple events locate away from the summit and possibly within the volcanic edifice ($z \le 1$ km). Figure 7b shows the location (red star) of a representative noneruptive event with an epicenter several

Figure 5. (a) Interior East Antarctica showing seismic stations (triangles) and seismicity (circles). The inset on the top left shows the location of the main map with respect to Antarctica. Event colors indicate moment magnitudes ($M_{\rm w}$) of the events as in the color bar. Red star represents the highlighted event location with waveforms shown in panel (b). This event has a magnitude ($M_{\rm w}$) of 1.4, and stations with picks are highlighted and named in panel (a). (b) Waveforms, plotted at respective source—station distances, filtered between 1 and 10 Hz for vertical and horizontal components. Yellow and red vertical lines indicate the P and S picks obtained with EQTransformer, respectively. The color version of this figure is available only in the electronic edition.

kilometers to the west of the summit with some of the stations that detect it. Figure 7c shows waveforms from the event in Figure 7b with P-wave and S-wave arrival estimates labeled. We obtained a preliminary depth of z = 6.9 km when we include all arrivals (P waves and S waves). However, the inferred direct S arrivals obtained with EQTransformer are likely to be dominated by nondirect S phase scattered energy as a consequence of the high scattering at Mount Erebus. When we only use Pwave arrivals to locate the event, we obtain a preliminary depth of $z = 0.21 \pm 3.26$ km, consistent with a shallow cryospheric event. We additionally looked for the controlled-source icehole shots from the 2008 Tomo Erebus experiment in our detections (Zandomeneghi et al., 2010) and found that 11 of the 15 (75 to 600 kg of mixed ammonium nitrate and fuel oil) events were detected. The four controlled-source events not in the catalog were likely near the ends of the Tomo Erebus profile and thus had azimuthal gaps exceeding the 270° cutoff. A more detailed analysis and interpretation of noneruptive events in the



Mount Erebus region will be the subject of a subsequent study using the catalog presented here as a starting point.

Discussion

This two-decade catalog shows multiple regions of Antarctica with widely varying rates of seismic activity (Figs. 1c and 2, Fig. S7) and reflects both seismic processes and a highly variable seismic station history and geometry. Previous studies (e.g., Winberry and Anandakrishnan, 2003; Winberry et al., 2009; Lough et al., 2013, 2015, 2018; Lucas et al., 2021) have noted seismic activity in most of these regions. However, the methodologies applied to detect and locate events in these and other studies are highly nonuniform, that is, manual inspection and quality control of waveforms, different implementations of short-term average/long-term average or other phase arrival detectors (Withers et al., 1998), phase association, velocity modeling, and other choices that may appreciably change the resulting catalogs. In contrast, our processing uniformly applies an automated workflow that includes (1) an ML phase detector (Mousavi et al., 2020) trained to detect earthquakes, mostly at distances less than 110 km and magnitudes less than 2.5, (2) a grid-search-based phase associator (Zhang et al., 2019), (3) a probabilistic location algorithm (Lomax et al., 2000, 2009) with quality control and uncertainty estimation, and (4) estimation of magnitudes (Satriano, 2022). Similar automated workflows have been applied successfully to other regions in the world to enhance or improve earthquake catalogs (Zhang et al., 2019; Wang et al., 2020; Garza-Giron et al., 2023; Yoon et al., 2023).

Based on the epicentral locations (Figs. 3a, 5a, 6a, and 7a) and initial waveform observations (Figs. 3b, 5b, 6b, and 7c), and previous detailed studies noted above, we suggest that the events in the seismic catalog encompass a wide variety of cryospheric, volcanic, magmatic, and tectonic sources. ML phase pickers (Ross *et al.*, 2018; Mousavi *et al.*, 2020) have been successfully applied and detect seismicity to illuminate

Figure 6. (a) Marie Byrd Land, showing seismic stations (triangles) and seismicity (circles). The inset on the bottom right shows the location of the main map with respect to Antarctica. Event colors indicate moment magnitudes (M_w) of the events as in the color bar. Red star represents the highlighted event location with waveforms shown in panel (b). This event has a magnitude of 1.7, an estimated depth of 32 km, and stations with picks are labeled in panel (a). (b) Waveforms showing an earthquake detected and located in Marie Byrd Land. Band-pass filtering (1-10 Hz) was applied for waveforms in vertical and horizontal components. Yellow and red vertical lines indicate the P and S picks obtained with EQTransformer, respectively. Waveforms are sorted by distance from the epicenter to each station. Earthquakes are located in or near the Thwaites Ice Shelf, Pine Island Glacier, and the Executive Committee Range. Deep longperiod seismicity located in the Executive Committee Range has been attributed to magmatic processes (Lough et al., 2013) within the Marie Byrd Land (dormant) volcanic province. The color version of this figure is available only in the electronic edition.

fault structures in Italy or California (Liu et al., 2020; Tan et al., 2021) or to image magmatic structures beneath volcanoes (Bannister et al., 2022; Wilding et al., 2023), but to our knowledge these new techniques have not been widely used to also detect large-scale cryoseismicity, which is abundant in Antarctica. The results here (Fig. 3) indicate that some cryoseismicity shares sufficiently similar waveform behavior (Smith, 2006; Hudson et al., 2020; Barcheck et al., 2021) with tectonic earthquakes that it can be recognized by an ML phase detector that has been trained solely on earthquakes. Currently, all the data sets (Mousavi et al., 2019; Michelini et al., 2021; Woollam et al., 2022) in use to train ML phase detectors solely utilize earthquake waveforms. Future research could incorporate training data sets consisting exclusively of icequake waveforms, which could enhance icequake detections to better monitor glacial dynamics in Antarctica, the Arctic, or in the alpine cryosphere.

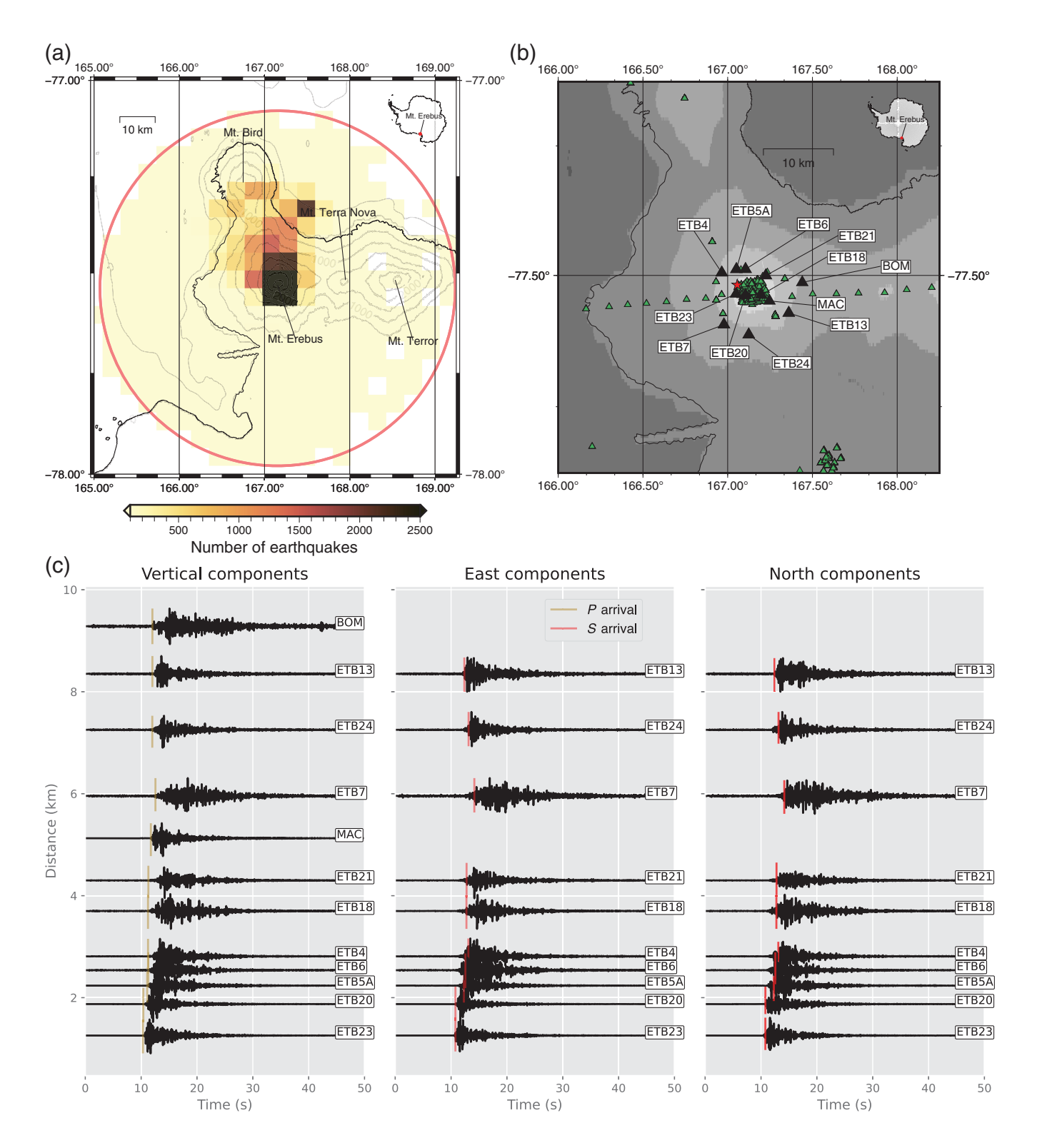


Figure 7. (a) Epicentral density for events on Mount Erebus. Inset on the top right shows the location of Mount Erebus with respect to Antarctica. Events located within the 50 km red circle are shown. 5 by 5 km regions indicate epicentral density. The dark and red regions have large numbers of events (n > 1500) and yellow regions have less than 500 events as indicated by the color bar. (b) Seismic stations (long-term and temporary) on Mount Erebus during the study period. Black triangles represent the stations that were installed during a noneruptive west flank (\sim 3 km east of the active crater) event highlighted with the red

star (estimated $M_{\rm w}$ 1.2; origin time 13 March 2008, 20:11:33 UTC). (c) Vertical and horizontal waveforms for the event shown in panel (b). Yellow and red vertical lines show the P- and S-wave arrivals obtained with EQTransformer, but the inferred S-wave arrivals are most likely nondirect S phase scattered energy characteristic of the highly scattered high-frequency seismograms recorded on the volcano. Waveforms are sorted by distance from the epicenter for each station. The color version of this figure is available only in the electronic edition.

Our seismic catalog contains 60,006 events with the majority of events concentrated in the Mount Erebus region (n = 47,961) or surrounding Ross Island (n = 10,619). This preponderance reflects both persistent seismicity and relatively dense and sustained seismic instrumentation there. The remainder of the continent shows a more modest level of activity (n = 1426) that reflects, both temporally and spatially, the deployment of temporary seismic networks. In some regions, such as East Antarctica, we detect fewer events than reported by prior and more specifically directed investigations. For instance, Lough et al. (2018) reported 27 events, where we report 12 (with 6 common detections). In other regions, such as central West Antarctica, we find 554 events, whereas Lucas et al. (2021) found 117 with 9 common detections. The smaller number of detections in East Antarctica (and other regions) might be explained by differing quality control criteria (location errors ≤ 50 km and azimuthal gap $\leq 270^{\circ}$). The azimuthal gap criteria culls a large number of events, including those occurring past the end of linear seismic deployments. Regions with a greater number of detections in this study, such as West Antarctica, are likely a consequence of applying an ML phase picker that identifies more phase arrivals than classic detectors. These differences suggest that there is more seismic activity than previously reported, but obtaining well-constrained hypocenters remains challenged by the sparse number, transient deployment, and wide spatial distribution of Antarctic seismic stations.

Basic methodological limitations in this catalog include: (1) we applied an ML phase picker, EQTransformer (Mousavi et al., 2020) trained with STEAD (Mousavi et al., 2019), which only includes tectonic events at local distances (<3°). Others ML seismic event detectors (Barkaoui et al., 2021; Steinmann et al., 2022) or training data sets (Cole et al., 2023; Suarez and Beroza, 2024) can help detect other uncatalogued seismicity at farther distances or events that do not generate impulsive P and S arrivals. (2) We used a global 1D velocity model (ak135, Kennett et al., 1995) in the association and location processing. Such a simple velocity model is not uniformly adequate across Antarctica, and we did not include station or topographic corrections, nor an ice layer. The inclusion of these refinements should increase the number of detections and/or improve hypocenter accuracy. (3) We applied specific quality control criteria in the association and location steps and a minimum SNR for magnitude estimation. These reduce the number of cataloged events but are intended to provide a higher quality catalog as a starting point for research that adapts to maximize/improve detections and associations and/or better characterize sources within a specific region. Other quality control criteria (e.g., Bondár et al., 2004; Michele et al., 2019) could be applied to influence the trade-off between the quantity of detection and hypocenter estimates. (4) The depths reported in the catalog are not well constrained in many cases, as corroborated by large depth errors. In general, to obtain a well-constrained hypocenter, it is necessary to have an *S*-wave arrival recorded within a distance of about 1.4 focal depths (Gomberg *et al.*, 1990). Such a requirement is not met by many events in the seismic catalog and depth estimates for events without proximal stations are very poorly constrained and must be interpreted cautiously. Depth estimates, where constrained, would also benefit from relocation with improved local velocity models and might help distinguish between different types of events depending on the region.

Acknowledging the limitations above, this Antarctic seismic catalog can be substantially improved in further studies. Here, we suggest a few possibilities: (1) the catalog events, or high-quality event subsets, could be used as the inputs for template-matching approaches (Gibbons and Ringdal, 2006; Shelly et al., 2007; Schaff, 2008) to increase the number of detections and in some cases enable relative relocation, or identification of temporally evolving seismicity trends. For example, template-matching approaches have proven helpful for constraining migrating effects of fluid injection-induced seismicity (Skoumal et al., 2015; Walter et al., 2018; Peña Castro et al., 2020; Glasgow et al., 2023) and seismicity near brittle-ductile transitional zones (Shelly, 2017; Ducellier and Creager, 2022). (2) Supervised deep learning phase pickers (Ross et al., 2018; Woollam et al., 2019; Zhu and Beroza, 2019; Mousavi et al., 2020) are becoming powerful tools to detect seismicity. However, any DL model can be challenged when encountering data with characteristics that are not represented in the training data set. Recent examples of relatively poor performance using DL pickers compared to human analyst results include a seismic sequence in Puerto Rico and seismic data from ocean-bottom seismic station in Alaska (Ruppert et al., 2023; Yoon et al., 2023). A practical way to improve DL picker performance in such cases is to use transfer learning (Pan and Yang, 2009), which applies a pretrained DL model in a substantially different setting. The task of the DL model is the same in the old and new settings (e.g., identifying phase arrivals) and the learned features from the old setting serve as a starting point. Subsequent training or tuning can be incrementally updated using a smaller amount of data from the new setting, allowing the DL model to learn more quickly and improve performance in the new setting (Chai et al., 2020; Lapins et al., 2021). Examples of successfully applied transfer learning in several settings, include local seismic data from an enhanced geothermal system in South Dakota (United States) and at Nabro volcano (Eritrea-Ethiopia border region), and showed that such an approach leads to a greater number of detections than the default pretrained DL phase pickers such as PhaseNet (Zhu and Beroza, 2019) or generalized seismic phase detection (Ross et al., 2018). Waveforms from the Antarctic seismic catalog might be used for a transfer learning approach to target specific regions and increase the number of detections. (3) Previous studies (Brodsky and van der Elst, 2014; Peng et al., 2014; Peña Castro et al., 2019; Li et al., 2021) have shown that the passage of teleseismic surface waves from large events

 $(M \ge 7)$ throughout the cryosphere and critically stressed fault systems can dynamically trigger instantaneous (or delayed) microearthquakes or icequakes. Figure S8 shows an increase in the number of seismic events near David Glacier and Mount Erebus after the occurrence of an M 7.7 teleseismic earthquake, suggesting that the seismic catalog might be a valuable starting point to investigate the occurrence of dynamic triggering in Antarctica. Another potential triggering interaction that could be studied with the catalog is cryoseismicity due to tidal and ocean swell stresses on ice shelves or marine-terminating glaciers (e.g., Aster et al., 2021, Olsen et al., 2021; Lucas et al., 2023b). (4) The seismic catalog contains signals from diverse source processes (icequakes, volcanic events, and tectonic earthquakes), as corroborated by an association with geologic/cryospheric provinces and results from prior studies, but we did not perform a systematic discrimination of the seismic signal types present in the catalog. Future research might focus on discriminating the seismic events present in the catalog by adapting discriminant algorithms (Hibert et al., 2017; Kong et al., 2022; Hourcade et al., 2023; Pirot et al., 2023). (5) Focal mechanisms or constraints (Hardebeck and Shearer, 2002, 2003; Pugh et al., 2016) could be obtained for some events with suitable azimuthal coverage, using P-wave polarities and S-/P-wave amplitude ratios, to infer the stress state and orientation of faults and their relationships to volcanic or tectonic provinces in Antarctica.

Summary

The new Antarctic seismic catalog in this study contains 60,006 events between magnitude $(M_{\rm w})$ -1.0 to 4.5. It was obtained using publicly available data from 2000 through 2020. The catalog was generated using a workflow that includes new and established software for earthquake detection (Mousavi et al., 2020; Woollam et al., 2022), association (Zhang et al., 2019), location (Lomax et al., 2000, 2009), and magnitude estimation (Satriano, 2022). Events in the catalog are located near the volcanoes, outlet glaciers, ice shelves, and within the continental interior. The catalog thus includes events from diverse source processes (cryospheric, volcanic, and tectonic). Preliminary observations include thousands of events near Mount Erebus, Ross Island, and the McMurdo Sound region, repeated seismic events at Ice Streams or large glaciers, and deep long-period events in Marie Byrd Land Executive Committee Range. We encourage the seismological community to make use of this exploratory catalog as a starting point to improve the understanding of Antarctic seismicity and its driving processes.

Data and Resources

The Antarctic seismic catalog is available at doi: 10.5281/zenodo .10710522 and will also be available at the U.S. Antarctic Program Data Center (USAP-DC, https://www.usap-dc.org/). The facilities of EarthScope Consortium were used for access to waveforms, related metadata, and/or derived products used in this study. These services are funded through the U.S. National Science Foundation (NSF)

Seismological Facility for the Advancement of Geoscience (SAGE) Award under Cooperative Agreement Number EAR-1724509. All seismic data were downloaded using EarthScope Consortium Webservices (https://service.iris.edu/). The Global Seismographic Network (GSN) is a cooperative scientific facility operated jointly by the NSF and the U.S. Geological Survey (USGS). The USGS earthquakes shown in Figure 1a can be obtained at doi: 10.5066/ F7MS3QZH. The NSF component is part of the NSF SAGE Facility, operated by EarthScope Consortium under Cooperative Agreement Number EAR-1724509. For a complete list of all seismic networks used in this study refer to the zenodo repository above. The data to all seismic events reported by the U.S. Geological Survey (USGS) between 1 January 2000 and 1 January 2021 were available at doi: 10.5066/F7MS3QZH. All the codes to build the catalog are open software. EQTransformer (Mousavi et al., 2020) is available using SeisBench (Woollam et al., 2022), rapid earthquake association and location (REAL) (Zhang et al., 2019) is available at https:// github.com/Dal-mzhang/REAL, NonLinLoc (Lomax et al., 2000) is available at https://github.com/alomax/NonLinLoc, and SourceSpec (Satriano, 2022) is available at https://github.com/SeismicSource/ sourcespec. Additional data processing and plotting were performed using the libraries ObsPy (Beyreuther et al., 2010), NumPy (Harris et al., 2020), pandas (The pandas Development Team, 2020), and ObsPlus (Chambers et al., 2021). All websites were last accessed in July 2024. The supplemental material contains 7 figures that complement our observations and analysis.

Declaration of Competing Interests

The authors acknowledge that there are no conflicts of interest recorded.

Acknowledgments

This research was supported by National Science Foundation Grant Numbers OPP-2023355, 1916978, 1744852, and 2346872. The authors thank Anya M. Reading, Alicia Hotovec-Ellis, an anonymous reviewer, the associate editor, and *SRL* Editor-in-Chief Allison Bent for their helpful comments. The University of New Mexico Center for Advanced Research Computing and National Science Foundation Grant Number EAR-2146272 provided high-performance computing resources. The authors thank many individuals and organizations who contributed to the design, deployment, and maintenance of Antarctic seismic stations throughout the years. Figures were generated using PyGMT (Tian *et al.*, 2023), a Python wrapper for the Generic Mapping Tools (GMT) (Wessel *et al.*, 2019), and Matplotlib (Hunter, 2007). Any use of trade, firm, or product names is for descriptive purposes only and does not imply endorsement by the U.S. Government.

References

Accardo, N. J., D. A. Wiens, S. Hernandez, R. C. Aster, A. Nyblade, A. Huerta, S. Anandakrishnan, T. Wilson, D. S. Heeszel, and I. W. Dalziel (2014). Upper mantle seismic anisotropy beneath the West Antarctic rift system and surrounding region from shear wave splitting analysis, *Geophys. J. Int.* 198, no. 1, 414–429.

Adams, R. (1969). Small earthquakes in Victoria land, Antarctica, *Nature* **224**, no. 5216, 255–256.

Adams, R., and A. Akoto (1986). Earthquakes in continental Antarctica, *J. Geodynam.* **6**, nos. 1/4, 263–270.

- Adams, R., A. Hughes, and B. Zhang (1985). A confirmed earthquake in continental Antarctica, *Geophys. J. Int.* **81**, no. 2, 489–492.
- Alley, R. B. (1993). In search of ice-stream sticky spots, *J. Glaciol.* **39**, no. 133, 447–454.
- Allstadt, K., and S. D. Malone (2014). Swarms of repeating stick-slip icequakes triggered by snow loading at Mount Rainier volcano, *J. Geophys. Res.* **119**, no. 5, 1180–1203.
- Anandakrishnan, S., D. Voigt, P. Burkett, B. Long, and R. Henry (2000). Deployment of a broadband seismic network in West Antarctica, *Geophys. Res. Lett.* 27, no. 14, 2053–2056.
- Anthony, R. E., R. C. Aster, D. Wiens, A. Nyblade, S. Anandakrishnan, A. Huerta, J. P. Winberry, T. Wilson, and C. Rowe (2015). The seismic noise environment of Antarctica, *Seismol. Res. Lett.* 86, no. 1, 89–100.
- Anthony, R. E., A. T. Ringler, M. DuVernois, K. R. Anderson, and D. C. Wilson (2021). Six decades of seismology at South Pole, Antarctica: Current limitations and future opportunities to facilitate new geophysical observations, *Seismol. Res. Lett.* 92, no. 5, 2718–2735.
- Aster, R., and J. P. Winberry (2017). Glacial seismology, *Rep. Progr. Phys.* **80**, 126801, doi: 10.1088/1361-6633/aa8473.
- Aster, R., W. MacIntosh, P. Kyle, R. Esser, B. Bartel, N. Dunbar, J. Johnson, R. Karstens, C. Kurnik, M. McGowan, et al. (2004). Real-time data received from Mount Erebus volcano, Antarctica, Eos Trans. AGU 85, no. 10, 97–101.
- Aster, R., S. Mah, P. Kyle, W. McIntosh, N. Dunbar, J. Johnson, M. Ruiz, and S. McNamara (2003). Very long period oscillations of Mount Erebus volcano, *J. Geophys. Res.* **108**, no. B11, doi: 10.1029/2002JB002101.
- Aster, R., D. Zandomeneghi, S. Mah, S. McNamara, D. Henderson, H. Knox, and K. Jones (2008). Moment tensor inversion of very long period seismic signals from Strombolian eruptions of Erebus volcano, J. Volcanol. Geotherm. Res. 177, no. 3, 635–647.
- Aster, R. C., B. P. Lipovsky, H. M. Cole, P. D. Bromirski, P. Gerstoft, A. Nyblade, D. A. Wiens, and R. Stephen (2021). Swell-triggered seismicity at the near-front damage zone of the Ross Ice Shelf, Seismol. Soc. Am. 92, no. 5, 2768–2792.
- Baker, M. G., R. C. Aster, R. E. Anthony, J. Chaput, D. A. Wiens, A. Nyblade, P. D. Bromirski, P. Gerstoft, and R. A. Stephen (2019). Seasonal and spatial variations in the ocean-coupled ambient wavefield of the Ross Ice Shelf, J. Glaciol. 65, no. 254, 912–925.
- Bannister, S., and B. Kennett (2002). Seismic activity in the transantarctic mountains-results from a broadband array deployment, *Terra Antartica* **9**, 41–46.
- Bannister, S., E. A. Bertrand, S. Heimann, S. Bourguignon, C. Asher, J. Shanks, and A. Harvison (2022). Imaging sub-caldera structure with local seismicity, Okataina volcanic centre, Taupo volcanic zone, using double-difference seismic tomography, *J. Volcanol. Geotherm. Res.* 431, 107653, doi: 10.1016/j.jvolgeores.2022.107653.
- Barcheck, G., E. Brodsky, P. Fulton, M. King, M. Siegfried, and S. Tulaczyk (2021). Migratory earthquake precursors are dominant on an ice stream fault, *Sci. Adv.* 7, no. 6, eabd0105, doi: 10.1126/sciadv.abd0105.
- Barkaoui, S., P. Lognonné, T. Kawamura, É. Stutzmann, L. Seydoux, M. V. de Hoop, R. Balestriero, J.-R. Scholz, G. Sainton, M. Plasman, et al. (2021). Anatomy of continuous Mars SEIS and pressure data from unsupervised learning, Bull. Seismol. Soc. Am. 111, no. 6, 2964–2981.

- Beeler, N. M., A. Thomas, R. Bürgmann, and D. Shelly (2013). Inferring fault rheology from low-frequency earthquakes on the San Andreas, J. Geophys. Res. 118, no. 11, 5976–5990.
- Bentley, C. R. (1987). Antarctic ice streams: A review, *J. Geophys. Res.* **92,** no. B9, 8843–8858.
- Bès de Berc, M., D. Zigone, P. Danecek, A. Steyer, F. Zanolin, A. Maggi, J. Thoré, A. Bernard, H. Blumentritt, S. Lambotte, et al. (2023). A new posthole seismometer at Concordia permanent research facility in the heart of the icy East Antarctic plateau, Seismol. Res. Lett. 95, 1518–1532.
- Beyreuther, M., R. Barsch, L. Krischer, T. Megies, Y. Behr, and J. Wassermann (2010). ObsPy: A Python toolbox for seismology, *Seismol. Res. Lett.* **81**, no. 3, 530–533.
- Bondár, I., S. C. Myers, E. R. Engdahl, and E. A. Bergman (2004). Epicentre accuracy based on seismic network criteria, *Geophys. J. Int.* 156, no. 3, 483–496.
- Brisbourne, A., G. Stuart, and J. P. O'Donnell (2016). 1D (2016-2018): UKANET: UK Antarctic Network, *International Federation of Digital Seismograph Networks* doi: 10.7914/SN/1D_2016.
- Brodsky, E. E., and N. J. van der Elst (2014). The uses of dynamic earthquake triggering, *Annu. Rev. Earth Planet. Sci.* 42, 317–339.
- Bromirski, P. D., A. Diez, P. Gerstoft, R. A. Stephen, T. Bolmer, D. Wiens, R. Aster, and A. Nyblade (2015). Ross ice shelf vibrations, *Geophys. Res. Lett.* **42**, 7589–7597.
- Cesca, S., M. Sugan, Ł. Rudzinski, S. Vajedian, P. Niemz, S. Plank, G. Petersen, Z. Deng, E. Rivalta, A. Vuan, et al. (2022). Massive earthquake swarm driven by magmatic intrusion at the Bransfield Strait, Antarctica, Commun. Earth Environ. 3, no. 1, 89, doi: 10.1038/s43247-022-00418-5.
- Chai, C., M. Maceira, H. J. Santos-Villalobos, S. V. Venkatakrishnan, M. Schoenball, W. Zhu, G. C. Beroza, C. Thurber, and , and EGS Collab Team (2020). Using a deep neural network and transfer learning to bridge scales for seismic phase picking, *Geophys. Res. Lett.* 47, no. 16, e2020GL088651, doi: 10.1029/ 2020GL088651.
- Chambers, D. J., M. S. Boltz, and C. J. Chamberlain (2021). ObsPlus: A pandas-centric ObsPy expansion pack, *J. Open Source Software* **6**, no. 60, 2696, doi: 10.21105/joss.02696.
- Chaput, J., R. Aster, A. D. Huerta, X. Sun, A. Lloyd, D. Wiens, A. Nyblade, S. Anandakrishan, J. P. Winberry, and T. Wilson (2014). The crustal thickness of West Antarctica, J. Geophys. Res. 119, 378–395.
- Chaput, J., M. Campillo, R. Aster, P. Roux, P. Kyle, H. Knox, and P. Czoski (2015). Multiple scattering from icequakes at Erebus volcano, Antarctica: Implications for imaging at glaciated volcanoes, *J. Geophys. Res.* 120, no. 2, 1129–1141.
- Chen, X., P. Shearer, F. Walter, and H. Fricker (2011). Seventeen Antarctic seismic events detected by global surface waves and a possible link to calving events from satellite images, *J. Geophys. Res.* **116**, no. B6, doi: 10.1029/2011JB008262.
- Chen, Z., P. Bromirski, P. Gerstoft, R. A. Stephen, W. Lee, S. Yun, S. Olinger, R. Aster, D. Wiens, and A. Nyblade (2019). Ross ice shelf icequakes associated with ocean gravity wave activity, *Geophys. Res. Lett.* 46, 8893–8902.
- Cole, H. M., W. L. Yeck, and H. M. Benz (2023). Mlaapde: A machine learning dataset for determining global earthquake source parameters, *Seismol. Res. Lett.* **94**, no. 5, 2489–2499.

- Danesi, S., S. Bannister, and A. Morelli (2007). Repeating earthquakes from rupture of an asperity under an Antarctic outlet glacier, *Earth Planet. Sci. Lett.* **253**, nos. 1/2, 151–158.
- DeSalvio, N. D., and W. Fan (2023). Ubiquitous earthquake dynamic triggering in southern California, *J. Geophys. Res.* **128**, no. 6, e2023JB026487, doi: 10.1029/2023JB026487.
- Dibble, R., P. Kyle, and C. Rowe (2008). Video and seismic observations of Strombolian eruptions at Erebus volcano, Antarctica, *J. Volcanol. Geotherm. Res.* **177**, no. 3, 619–634.
- Ducellier, A., and K. C. Creager (2022). An 8-year-long low-frequency earthquake catalog for southern Cascadia, *J. Geophys. Res.* **127**, no. 4, e2021JB022986, doi: 10.1029/2021JB022986.
- Ekstrom, G., M. Nettles, and G. A. Abers (2003). Glacial earthquakes, *Science* **302**, no. 5645, 622–624.
- Evison, F. (1967). Note on the aseismicity of Antarctica, *New Zeal. J. Geol. Geophys.* **10**, no. 2, 479–483.
- Font, Y., H. Kao, S. Lallemand, C.-S. Liu, and L.-Y. Chiao (2004). Hypocentre determination offshore of eastern Taiwan using the maximum intersection method, *Geophys. J. Int.* 158, no. 2, 655–675.
- Gambino, S., and E. Privitera (1994). Characterization of earthquakes recorded by Mt. Melborne volcano seismic network (northern Victoria Land, Antarctica), *Terra Antarctica* 1, 167–172.
- Gambino, S., and E. Privitera (1996). Mt. Melbourne volcano, Antarctica: Evidence of seismicity related to volcanic activity, *Pure Appl. Geophys.* 146, 305–318.
- Garza-Giron, R., E. E. Brodsky, Z. J. Spica, M. M. Haney, and P. W. Webley (2023). A specific earthquake processing workflow for studying long-lived, explosive volcanic eruptions with application to the 2008 Okmok volcano, Alaska, eruption, *J. Geophys. Res.* doi: 10.1029/2022JB025882.
- Gerst, A., M. Hort, R. C. Aster, J. B. Johnson, and P. R. Kyle (2013). The first second of volcanic eruptions from the Erebus volcano lava lake, Antarctica-Energies, pressures, seismology, and infrasound, *J. Geophys. Res.* **118**, no. 7, 3318–3340.
- Gibbons, S. J., and F. Ringdal (2006). The detection of low magnitude seismic events using array-based waveform correlation, *Geophys. J. Int.* **165**, no. 1, 149–166.
- Glasgow, M. E., B. Schmandt, and S. L. Bilek (2023). Cascading multi-segment rupture in an injection-induced earthquake sequence with a $M_{\rm w}$ 5.3 mainshock, *Earth Planet. Sci. Lett.* **620,** 118335, doi: 10.1016/j.epsl.2023.118335.
- Gomberg, J. S., K. M. Shedlock, and S. W. Roecker (1990). The effect of S-wave arrival times on the accuracy of hypocenter estimation, *Bull. Seismol. Soc. Am.* 80, no. 6A, 1605–1628.
- Gräff, D., and F. Walter (2021). Changing friction at the base of an alpine glacier, *Sci. Rep.* **11**, no. 1, 10872, doi: 10.1038/s41598-021-90176-9.
- Gräff, D., M. Köpfli, B. P. Lipovsky, P. A. Selvadurai, D. Farinotti, and F. Walter (2021). Fine structure of microseismic glacial stick-slip, *Geophys. Res. Lett.* 48, no. 22, e2021GL096043, doi: 10.1029/ 2021GL096043.
- Hammer, C., M. Ohrnberger, and V. Schlindwein (2015). Pattern of cryospheric seismic events observed at Ekström Ice Shelf, Antarctica, *Geophys. Res. Lett.* **42**, no. 10, 3936–3943.
- Hansen, S. E., J. H. Graw, L. M. Kenyon, A. A. Nyblade, D. A. Wiens,
 R. C. Aster, A. D. Huerta, S. Anandakrishnan, and T. Wilson (2014). Imaging the Antarctic mantle using adaptively

- parameterized *P*-wave tomography: Evidence for heterogeneous structure beneath West Antarctica, *Earth Planet. Sci. Lett.* **408**, 66–78.
- Hansen, S. E., J. Julia, A. A. Nyblade, M. L. Pyle, D. A. Wiens, and S. Anandakrishnan (2009). Using S wave receiver functions to estimate crustal structure beneath ice sheets: An application to the Transantarctic Mountains and East Antarctic craton, *Geochem. Geophys. Geosyst.* 10, no. 8, doi: 10.1029/2009GC002576.
- Hansen, S. E., A. A. Nyblade, D. S. Heeszel, D. A. Wiens, P. Shore, and M. Kanao (2010). Crustal structure of the Gamburtsev Mountains, East Antarctica, from S-wave receiver functions and Rayleigh wave phase velocities, *Earth Planet. Sci. Lett.* **300**, nos. 3/4, 395–401.
- Hansen, S. E., A. M. Reusch, T. Parker, D. K. Bloomquist, P. Carpenter, J. H. Graw, and G. R. Brenn (2015). The Transantarctic Mountains Northern Network (TAMNNET): Deployment and performance of a seismic array in Antarctica, Seismol. Res. Lett. 86, no. 6, 1636–1644.
- Hardebeck, J. L., and P. M. Shearer (2002). A new method for determining first-motion focal mechanisms, *Bull. Seismol. Soc. Am.* 92, no. 6, 2264–2276.
- Hardebeck, J. L., and P. M. Shearer (2003). Using S/P amplitude ratios to constrain the focal mechanisms of small earthquakes, *Bull. Seismol. Soc. Am.* **93**, no. 6, 2434–2444.
- Harris, C. R., K. J. Millman, S. J. Van Der Walt, R. Gommers, P. Virtanen, D. Cournapeau, E. Wieser, J. Taylor, S. Berg, N. J. Smith, et al. (2020). Array programming with NumPy, Nature 585, no. 7825, 357–362.
- Heeszel, D. S., H. A. Fricker, J. N. Bassis, S. O'Neel, and F. Walter (2014). Seismicity within a propagating ice shelf rift: The relationship between icequake locations and ice shelf structure, *J. Geophys. Res.* **119**, no. 4, 731–744.
- Hibert, C., F. Provost, J.-P. Malet, A. Maggi, A. Stumpf, and V. Ferrazzini (2017). Automatic identification of rockfalls and volcano-tectonic earthquakes at the Piton de la Fournaise volcano using a Random Forest algorithm, J. Volcanol. Geotherm. Res. 340, 130–142
- Hourcade, C., M. Bonnin, and É. Beucler (2023). New CNN-based tool to discriminate anthropogenic from natural low magnitude seismic events, *Geophys. J. Int.* **232**, no. 3, 2119–2132.
- Huang, M.-H., K. Udell Lopez, and K. G. Olsen (2022). Icequake-magnitude scaling relationship along a rift within the Ross Ice Shelf, Antarctica, *Geophys. Res. Lett.* 49, no. 10, e2022GL097961, doi: 10.1029/2022GL097961.
- Hudson, T., S. Kufner, A. Brisbourne, J. Kendall, A. Smith, R. Alley, R. Arthern, and T. Murray (2023). Highly variable friction and slip observed at Antarctic ice stream bed, *Nature Geosci.* 16, 612–618.
- Hudson, T. S., A. F. Baird, J.-M. Kendall, S.-K. Kufner, A. M. Brisbourne, A. M. Smith, A. Butcher, A. Chalari, and A. Clarke (2021). Distributed acoustic sensing (DAS) for natural microseismicity studies: A case study from Antarctica, *J. Geophys. Res.* 126, no. 7, e2020JB021493, doi: 10.1029/2020JB021493.
- Hudson, T. S., A. M. Brisbourne, F. Walter, D. Gräff, R. S. White, and A. M. Smith (2020). Icequake source mechanisms for studying glacial sliding, *J. Geophys. Res.* 125, no. 11, e2020JF005627, doi: 10.1029/2020JF005627.
- Hunter, J. D. (2007). Matplotlib: A 2d graphics environment, Comput. Sci. Eng. 9, no. 3, 90–95.

- Johnston, A. C. (1987). Suppression of earthquakes by large continental ice sheets, *Nature* 330, no. 6147, 467–469.
- Johnston, A. C. (1989). *The Effect of Large Ice Sheets on Earthquake Genesis*, Springer Netherlands, Dordrecht, 581–599.
- Kaminuma, K., M. Baba, and S. Ukei (1986). Earthquake swarms on Mt. Erebus, Antartica, *J. Geodynam.* **6**, 391–404.
- Kaminuma, K., S. Ueki, and K. Juergen (1985). Volcanic earthquake swarms at Mt. Erebus, Antarctica, *Tectonophysics* 114, nos. 1/4, 357–369.
- Kanao, M. (2014). Seismicity in the Antarctic continent and surrounding ocean, *Open J. Earthq. Res.* 3, no. 1, 5–14.
- Kennett, B. L., E. Engdahl, and R. Buland (1995). Constraints on seismic velocities in the Earth from travel times, *Geophys. J. Int.* 122, no. 1, 108–124.
- Knox, H., J. Chaput, R. Aster, and P. Kyle (2018). Multiyear shallow conduit changes observed with lava lake eruption seismograms at Erebus volcano, Antarctica, J. Geophys. Res. 123, no. 4, 3178–3196.
- Kong, Q., R. Wang, W. R. Walter, M. Pyle, K. Koper, and B. Schmandt (2022). Combining deep learning with physics based features in explosion-earthquake discrimination, *Geophys. Res. Lett.* 49, no. 13, e2022GL098645, doi: 10.1029/2022GL098645.
- Kufner, S.-K., A. M. Brisbourne, A. M. Smith, T. S. Hudson, T. Murray, R. Schlegel, J. M. Kendall, S. Anandakrishnan, and I. Lee (2021). Not all icequakes are created equal: Basal icequakes suggest diverse bed deformation mechanisms at Rutford Ice Stream, West Antarctica, J. Geophys. Res. 126, no. 3, e2020JF006001, doi: 10.1029/2020JF006001.
- Lamb, O. D., J. M. Lees, L. F. Marin, J. Lazo, A. Rivera, M. J. Shore, and S. J. Lee (2020). Investigating potential icequakes at Llaima volcano, Chile, *Volcanica* 3, no. 1, doi: 10.30909/vol.03.01.2942.
- Lander, J. F. (1959). Seismicity of Antarctica and Guam, *Seismol. Res. Lett.* **30**, no. 2, 16–17.
- Lander, J. F. (1962). Seismicity of Antarctica, *Master's Thesis*, American University.
- Lapins, S., B. Goitom, J.-M. Kendall, M. J. Werner, K. V. Cashman, and J. O. Hammond (2021). A little data goes a long way: Automating seismic phase arrival picking at Nabro volcano with transfer learning, *J. Geophys. Res.* 126, no. 7, e2021JB021910, doi: 10.1029/2021JB021910.
- Lawrence, J. F., D. A. Wiens, A. A. Nyblade, S. Anandakrishnan, P. J. Shore, and D. Voigt (2006a). Crust and upper mantle structure of the Transantarctic Mountains and surrounding regions from receiver functions, surface waves, and gravity: Implications for uplift models, Geochem. Geophys. Geosys. 7, no. 10, doi: 10.1029/2006GC001282.
- Lawrence, J. F., D. A. Wiens, A. A. Nyblade, S. Anandakrishnan, P. J. Shore, and D. Voigt (2006b). Rayleigh wave phase velocity analysis of the Ross Sea, Transantarctic Mountains, and East Antarctica from a temporary seismograph array, *J. Geophys. Res.* 111, no. B6, doi: 10.1029/2005JB003812.
- Lay, T., and H. Kanamori (1981). An asperity model of large earth-quake sequences, in *Earthquake Prediction: An International Review*, D. W. Simpson and P. G. Simpson (Editors), Vol. 4, American Geophysical Union, Washington D.C., 579–592.
- Leroy, N., M. Vallée, D. Zigone, B. Romanowicz, E. Stutzmann, A. Maggi, C. Pardo, J. P. Montagner, M. Bes de Berc, C. Broucke, et al. (2023). GEOSCOPE Network: 40 yr of global broadband seismic data, Seismol. Res. Lett. 95, 1495–1517.

- Li, C., Z. Peng, J. A. Chaput, J. I. Walter, and R. C. Aster (2021). Remote triggering of icequakes at Mt. Erebus, Antarctica by large teleseismic earthquakes, *Seismol. Res. Lett.* 92, no. 5, 2866–2875.
- Liu, M., M. Zhang, W. Zhu, W. L. Ellsworth, and H. Li (2020). Rapid characterization of the July 2019 Ridgecrest, California, earthquake sequence from raw seismic data using machine-learning phase picker, *Geophys. Res. Lett.* 47, no. 4, e2019GL086189, doi: 10.1029/2019GL086189.
- Lomax, A. (2005). A reanalysis of the hypocentral location and related observations for the great 1906 California earthquake, *Bull. Seismol. Soc. Am.* **95**, no. 3, 861–877.
- Lomax, A. (2008). Location of the focus and tectonics of the focal region of the California earthquake of 18 April 1906, Bull. Seismol. Soc. Am. 98, no. 2, 846–860.
- Lomax, A., A. Michelini, A. Curtis, and R. Meyers (2009). Earthquake location, direct, global-search methods, in *Encyclopedia of Complexity and Systems Science*, R. Meyers (Editor), Springer, New York, New York, Vol. 5, 2449–2473.
- Lomax, A., J. Virieux, P. Volant, and C. Berge-Thierry (2000). Probabilistic earthquake location in 3D and layered models: Introduction of a Metropolis-Gibbs method and comparison with linear locations, in *Advances in Seismic Event Location*, C. H. Thurber and N. Rabinowitz (Editors), Springer, Dordrecht, 101–134.
- Lombardi, D., I. Gorodetskaya, G. Barruol, and T. Camelbeeck (2019). Thermally induced icequakes detected on blue ice areas of the East Antarctic ice sheet, *Ann. Glaciol.* **60**, no. 79, 45–56.
- Lough, A. C., C. G. Barcheck, D. A. Wiens, A. Nyblade, and S. Anandakrishnan (2015). A previously unreported type of seismic source in the firn layer of the East Antarctic ice sheet, *J. Geophys. Res.* 120, no. 11, 2237–2252.
- Lough, A. C., D. A. Wiens, C. Grace Barcheck, S. Anandakrishnan, R. C. Aster, D. D. Blankenship, A. D. Huerta, A. Nyblade, D. A. Young, and T. J. Wilson (2013). Seismic detection of an active subglacial magmatic complex in Marie Byrd Land, Antarctica, *Nature Geosci.* 6, no. 12, 1031–1035.
- Lough, A. C., D. A. Wiens, and A. Nyblade (2018). Reactivation of ancient Antarctic rift zones by intraplate seismicity, *Nature Geosci.* 11, no. 7, 515–519.
- Lucas, E. M., A. A. Nyblade, R. C. Aster, D. A. Wiens, T. J. Wilson, J. P. Winberry, and A. D. Huerta (2023a). Tidally modulated glacial seismicity at the Foundation Ice Stream, West Antarctica, J. Geophys. Res. 128, no. 7, doi: 10.1029/2023JF007172.
- Lucas, E. M., A. A. Nyblade, R. C. Aster, D. A. Wiens, T. J. Wilson, J. P. Winberry, and A. D. Huerta (2023b). Tidally modulated glacial seismicity at the Foundation Ice Stream, West Antarctica, *J. Geophys. Res.* 128, no. 7, e2023JF007172, doi: 10.1029/2023JF007172.
- Lucas, E. M., A. A. Nyblade, A. J. Lloyd, R. C. Aster, D. A. Wiens, J. P. O'Donnell, G. W. Stuart, T. J. Wilson, I. W. Dalziel, J. P. Winberry, et al. (2021). Seismicity and Pn velocity structure of central West Antarctica, Geochem. Geophys. Geosys. 22, no. 2, e2020GC009471, doi: 10.1029/2020GC009471.
- MacAyeal, D. R., E. A. Okal, R. C. Aster, and J. Bassis (2008). Seismic and hydroacoustic tremor generated by colliding icebergs, *J. Geophys. Res.* **113**, no. F3, doi: 10.1029/2008JF001005.
- Martin, S., R. Drucker, R. Aster, F. Davey, E. Okal, T. Scambos, and D. MacAyeal (2010). Kinematic and seismic analysis of giant tabular

- iceberg breakup at Cape Adare, Antarctica, *J. Geophys. Res.* **115**, doi: 10.1029/2009JB006700.
- Mayewski, P. A., M. Meredith, C. Summerhayes, J. Turner, A. Worby, P. Barrett, G. Casassa, N. A. Bertler, T. Bracegirdle, A. Naveira Garabato, *et al.* (2009). State of the Antarctic and Southern Ocean climate system, *Rev. Geophys.* 47, no. 1, doi: 10.1029/2007RG000231.
- Michele, M., D. Latorre, and A. Emolo (2019). An empirical formula to classify the quality of earthquake locations, *Bull. Seismol. Soc. Am.* **109**, no. 6, 2755–2761.
- Michelini, A., S. Cianetti, S. Gaviano, C. Giunchi, D. Jozinović, and V. Lauciani (2021). Instance–The Italian seismic dataset for machine learning, *Earth Syst. Sci. Data* 13, no. 12, 5509–5544.
- Minowa, M., E. A. Podolskiy, and S. Sugiyama (2019). Tide-modulated ice motion and seismicity of a floating glacier tongue in East Antarctica, *Ann. Glaciol.* **60**, no. 79, 57–67.
- Mousavi, S. M., W. L. Ellsworth, W. Zhu, L. Y. Chuang, and G. C. Beroza (2020). Earthquake transformer–An attentive deep-learning model for simultaneous earthquake detection and phase picking, *Nat. Commun.* 11, no. 1, 3952, doi: 10.1038/s41467-020-17591-w.
- Mousavi, S. M., Y. Sheng, W. Zhu, and G. C. Beroza (2019). Stanford earthquake dataset (STEAD): A global data set of seismic signals for AI, *IEEE Access* 7, 179,464–179,476.
- Muller, C., V. Schlindwein, A. Eckstaller, and H. Miller (2005).Singing icebergs, Science 310, no. 5752, 1299–1299.
- Münchmeyer, J., J. Woollam, A. Rietbrock, F. Tilmann, D. Lange, T. Bornstein, T. Diehl, C. Giunchi, F. Haslinger, D. Jozinović, *et al.* (2022). Which picker fits my data? A quantitative evaluation of deep learning based seismic pickers, *J. Geophys. Res.* **127**, no. 1, e2021JB023499, doi: 10.1029/2021JB023499.
- Nettles, M., and G. Ekström (2010). Glacial earthquakes in Greenland and Antarctica, *Annu. Rev. Earth Planet. Sci.* **38**, 467–491.
- Nøst, O. A. (2004). Measurements of ice thickness and seabed topography under the Fimbul Ice Shelf, Dronning Maud Land, Antarctica, *J. Geophys. Res.* **109**, no. C10, doi: 10.1029/2004JC002277.
- Oborina, S., and A. Sytinskiy (1978). The Aantarctic earthquake of Oct. 15, 1974, *Polar Geogr.* 2, no. 2, 97–99.
- Olinger, S., P. Lipovsky Bradley, D. Wiens, R. Aster, P. Bromirski, Z. Chen, P. Gerstoft, A. Nyblade, and R. A. Stephen (2019). Tidal and thermal stresses drive seismicity along a major Ross Ice Shelf rift, *Geophys. Res. Lett.* 46, 6644–6652.
- Olivet, J. L., L. S. Bettucci, O. A. Castro-Artola, H. Castro, M. Rodrguez, and E. Latorres (2021). A seismic swarm at the Bransfield rift, Antarctica, *J. South Am. Earth Sci.* 111, 103412, doi: 10.1016/j.jsames.2021.103412.
- Olsen, K. G., T. A. Hurford, N. C. Schmerr, M.-H. Huang, K. M. Brunt, S. Zipparo, H. M. Cole, and R. C. Aster (2021). Projected seismic activity at the Tiger stripe fractures on Enceladus, Saturn, from an analog study of tidally modulated icequakes within the Ross Ice Shelf, Antarctica, J. Geophys. Res. 126, no. 6, e2021JE006862, doi: 10.1029/2021JE006862.
- O'Neel, S., H. P. Marshall, D. E. McNamara, and W. T. Pfeffer (2007). Seismic detection and analysis of icequakes at Columbia Glacier, Alaska, *J. Geophys. Res.* 112, no. F3, doi: 10.1029/2006JF000595.
- Pan, S. J., and Q. Yang (2009). A survey on transfer learning, *IEEE Trans. Knowl. Data Eng.* **22,** no. 10, 1345–1359.

- Panter, K., W. McIntosh, and J. Smellie (1994). Volcanic history of Mount Sidley, a major alkaline volcano in Marie Byrd Land, Antarctica, Bull. Volcanol. 56, 361–376.
- Park, Y., H. J. Yoo, W. S. Lee, J. Lee, Y. Kim, S.-H. Lee, D. Shin, and H. Park (2014). Deployment and performance of a broadband seismic network near the new Korean Jang Bogo research station, Terra Nova Bay, East Antarctica, Seismol. Res. Lett. 85, no. 6, 1341–1347.
- Paul Winberry, J., S. Anandakrishnan, D. A. Wiens, and R. B. Alley (2013). Nucleation and seismic tremor associated with the glacial earthquakes of Whillans Ice Stream, Antarctica, *Geophys. Res. Lett.* 40, no. 2, 312–315.
- Peña Castro, A., S. L. Dougherty, R. Harrington, and E. S. Cochran (2019). Delayed dynamic triggering of disposal-induced earth-quakes observed by a dense array in northern Oklahoma, *J. Geophys. Res.* **124,** no. 4, 3766–3781.
- Peña Castro, A., M. Roth, A. Verdecchia, J. Onwuemeka, Y. Liu, R. Harrington, Y. Zhang, and H. Kao (2020). Stress chatter via fluid flow and fault slip in a hydraulic fracturing-induced earthquake sequence in the Montney Formation, British Columbia, *Geophys. Res. Lett.* 47, no. 14, e2020GL087254, doi: 10.1029/2020GL087254.
- Peng, Z., J. I. Walter, R. C. Aster, A. Nyblade, D. A. Wiens, and S. Anandakrishnan (2014). Antarctic icequakes triggered by the 2010 Maule earthquake in Chile, *Nature Geosci.* 7, no. 9, 677–681.
- Pham, T.-S., and H. Tkalčić (2018). Antarctic ice properties revealed from teleseismic P wave coda autocorrelation, *J. Geophys. Res.* **123**, no. 9, 7896–7912.
- Pirot, E., C. Hibert, and A. Mangeney (2023). Enhanced glacial earthquake catalogs with supervised machine learning for more comprehensive analysis, *Geophys. J. Int.* **236**, 849–871.
- Podolskiy, E. A., and F. Walter (2016). Cryoseismology, *Rev. Geophys.* **54,** no. 4, 708–758.
- Poli, P. (2023). Continuation of events detection with global longperiod seismic data: An analysis from 2010 to 2022, *Seismol. Res. Lett.* **95**, 1486–1494.
- Poli, P., L. Cabrera, M. Flores, J. Báez, J. Ammirati, J. Vásquez, and S. Ruiz (2022). Volcanic origin of a long-lived swarm in the central Bransfield basin, Antarctica, *Geophys. Res. Lett.* 49, no. 1, e2021GL095447, doi: 10.1029/2021GL095447.
- Pugh, D., R. White, and P. Christie (2016). A Bayesian method for microseismic source inversion, *Geophys. J. Int.* 206, no. 2, 1009–1038.
- Pyle, M. L., D. A. Wiens, A. A. Nyblade, and S. Anandakrishnan (2010). Crustal structure of the Transantarctic Mountains near the Ross Sea from ambient seismic noise tomography, *J. Geophys. Res.* 115, no. B11, doi: 10.1029/2009JB007081.
- Qamar, A. (1988). Calving icebergs: A source of low-frequency seismic signals from Columbia Glacier, Alaska, J. Geophys. Res. 93, no. B6, 6615–6623.
- Reading, A. (2002). Antarctic seismicity and neotectonics, *R. Soc. New Zeal. Bull.* **35,** 479–484.
- Reading, A. M. (2007). *The Seismicity of the Antarctic Plate*, Vol. 425, GSA Special Papers, Golden, Colorado, 285–298, doi: 10.1130/SPE425.
- Rial, J. A., C. Tang, and K. Steffen (2009). Glacial rumblings from Jakobshavn ice stream, Greenland, J. Glaciol. 55, no. 191, 389–399.
- Richardson, J. P., G. P. Waite, W. D. Pennington, R. M. Turpening, and J. M. Robinson (2012). Icequake locations and discrimination of source

- and path effects with small aperture arrays, Bering Glacier terminus, AK, *J. Geophys. Res.* **117,** no. F4, doi: 10.1029/2012JF002405.
- Rignot, E., J. Mouginot, and B. Scheuchl (2017). MEaSUREs InSARbased Antarctica ice velocity map, version 2, doi: 10.5067/D7GK8F5J8M8R.
- Ringler, A. T., R. E. Anthony, R. C. Aster, C. J. Ammon, S. Arrowsmith, H. Benz, C. Ebeling, A. Frassetto, W.-Y. Kim, P. Koelemeijer, et al. (2022). Achievements and prospects of global broadband seismographic networks after 30 years of continuous geophysical observations, Rev. Geophys. 60, no. 3, e2021RG000749, doi: 10.1029/ 2021RG000749.
- Röösli, C., F. Walter, S. Husen, L. C. Andrews, M. P. Lüthi, G. A. Catania, and E. Kissling (2014). Sustained seismic tremors and icequakes detected in the ablation zone of the Greenland ice sheet, *J. Glaciol.* 60, no. 221, 563–575.
- Ross, Z. E., M.-A. Meier, E. Hauksson, and T. H. Heaton (2018). Generalized seismic phase detection with deep learning, *Bull. Seismol. Soc. Am.* 108, no. 5A, 2894–2901.
- Rouland, D., C. Condis, C. Parmentier, and A. Souriau (1992).
 Previously undetected earthquakes in the southern hemisphere located using long-period Geoscope data, *Bull. Seismol. Soc. Am.* 82, no. 6, 2448–2463.
- Rouland, D., C. Condis, and G. Roult (2003). Overlooked earthquakes on and around the Antarctica plate: Identification and location of 1999 shallow depth events, *Tectonophysics* **376**, nos. 1/2, 1–17.
- Rowe, C., R. Aster, P. Kyle, R. Dibble, and J. Schlue (2000). Seismic and acoustic observations at Mount Erebus volcano, Ross Island, Antarctica, 1994–1998, J. Volcanol. Geotherm. Res. 101, nos. 1/2, 105–128.
- Ruppert, N. A., G. Barcheck, and G. A. Abers (2023). Enhanced regional earthquake catalog with Alaska amphibious community seismic experiment data, *Seismol. Soc. Am.* **94**, no. 1, 522–530.
- Salvini, F., and F. Storti (1999). Cenozoic tectonic lineaments of the Terra Nova Bay region, Ross embayment, Antarctica, *Global Planet. Change* **23**, nos. 1/4, 129–144.
- Satriano, C. (2022). SourceSpec—Earthquake source parameters from *P* or *S*-wave displacement spectra, *Zenodo*, doi: 10.1093/gji/ggab159.
- Sawi, T., B. Holtzman, F. Walter, and J. Paisley (2022). An unsupervised machine-learning approach to understanding seismicity at an alpine glacier, *J. Geophys. Res.* **127**, no. 12, e2022JF006909, doi: 10.1029/2022JF006909.
- Schaff, D. P. (2008). Semiempirical statistics of correlation-detector performance, *Bull. Seismol. Soc. Am.* **98**, no. 3, 1495–1507.
- Schweitzer, J., M. Pirli, M. Roth, and T. Kværna (2014). Troll: A new, very broadband seismic station in Antarctica, *Seismol. Res. Lett.* **85**, no. 4, 852–862.
- Sergienko, O. V., and C. L. Hulbe (2011). 'Sticky spots' and subglacial lakes under ice streams of the Siple Coast, Antarctica, *Ann. Glaciol.* 52, no. 58, 18–22.
- Shelly, D. R. (2017). A 15-year catalog of more than 1 million low-frequency earthquakes: Tracking tremor and slip along the deep San Andreas fault, *J. Geophys. Res.* **122**, no. 5, 3739–3753.
- Shelly, D. R., G. C. Beroza, and S. Ide (2007). Non-volcanic tremor and low-frequency earthquake swarms, *Nature* 446, no. 7133, 305–307.
- Shen, W., D. A. Wiens, S. Anandakrishnan, R. C. Aster, P. Gerstoft, P. D. Bromirski, S. E. Hansen, I. W. Dalziel, D. S. Heeszel, A. D.

- Huerta, *et al.* (2018). The crust and upper mantle structure of central and West Antarctica from Bayesian inversion of Rayleigh wave and receiver functions, *J. Geophys. Res.* **123**, no. 9, 7824–7849.
- Sims, K. W. W., R. C. Aster, G. Gaetani, J. Blichert-Toft, E. H. Phillips, P. J. Wallace, G. S. Mattioli, D. Rasmussen, and E. S. Boyd (2021). *Chapter 7.2 Mount Erebus*, Geological Society, London, Memoirs, London.
- Skoumal, R. J., M. R. Brudzinski, and B. S. Currie (2015). Distinguishing induced seismicity from natural seismicity in Ohio: Demonstrating the utility of waveform template matching, J. Geophys. Res. 120, no. 9, 6284–6296.
- Smith, A. (2006). Microearthquakes and subglacial conditions, *Geophys. Res. Lett.* **33**, no. 24, doi: 10.1029/2006GL028207.
- Smith, E., A. Smith, R. White, A. Brisbourne, and H. Pritchard (2015).
 Mapping the ice-bed interface characteristics of Rutford Ice Stream, West Antarctica, using microseismicity, J. Geophys. Res. 120, no. 9, 1881–1894.
- Steinmann, R., L. Seydoux, E. Beaucé, and M. Campillo (2022). Hierarchical exploration of continuous seismograms with unsupervised learning, *J. Geophys. Res.* **127**, no. 1, e2021JB022455, doi: 10.1029/2021JB022455.
- Suarez, A. L. A., and G. Beroza (2024). Curated regional earthquake waveforms (crew) dataset, *Seismica* 3, no. 1, doi: 10.26443/seismica.y3i1.1049.
- Sykes, L. R. (1978). Intraplate seismicity, reactivation of preexisting zones of weakness, alkaline magmatism, and other tectonism postdating continental fragmentation, *Rev. Geophys.*, **16**, no. 4, 621–688
- Talwani, P. (2014). Intraplate Earthquakes, Cambridge University Press, New York.
- Tan, Y. J., F. Waldhauser, W. L. Ellsworth, M. Zhang, W. Zhu, M. Michele, L. Chiaraluce, G. C. Beroza, and M. Segou (2021). Machine-learning-based high-resolution earthquake catalog reveals how complex fault structures were activated during the 2016–2017 central Italy sequence, Seism. Rec. 1, no. 1, 11–19.
- The pandas Development Team (2020). pandas-dev/pandas: Pandas (software), available at https://github.com/pandas-dev/pandas (last accessed July 2024).
- Tian, D., L. Uieda, W. J. Leong, W. Schlitzer, Y. Fröhlich, M. Grund, M. Jones, L. Toney, J. Yao, Y. Magen, et al. (2023). PyGMT: A Python interface for the Generic Mapping Tools, Zenodo, doi: 10.5281/zenodo.4592991.
- Van Wyk de Vries, M., R. G. Bingham, and A. S. Hein (2018). A New Volcanic Province: An Inventory of Subglacial Volcanoes in West Antarctica, Vol. 461, Geological Society, Special Publications, London, 231–248.
- Walter, F., J. F. Clinton, N. Deichmann, D. S. Dreger, S. E. Minson, and M. Funk (2009). Moment tensor inversions of icequakes on Gornergletscher, Switzerland, *Bull. Seismol. Soc. Am.* 99, no. 2A, 852–870.
- Walter, F., N. Deichmann, and M. Funk (2008). Basal icequakes during changing subglacial water pressures beneath Gornergletscher, Switzerland, *J. Glaciol.* **54**, no. 186, 511–521.
- Walter, J. I., C. Frohlich, and T. Borgfeldt (2018). Natural and induced seismicity in the Texas and Oklahoma Panhandles, Seismol. Res. Lett. 89, no. 6, 2437–2446.

- Wang, R., B. Schmandt, M. Zhang, M. Glasgow, E. Kiser, S. Rysanek, and R. Stairs (2020). Injection-induced earthquakes on complex fault zones of the Raton basin illuminated by machine-learning phase picker and dense nodal array, *Geophys. Res. Lett.* 47, no. 14, e2020GL088168, doi: 10.1029/2020GL088168.
- Watson, T., A. Nyblade, D. A. Wiens, S. Anandakrishnan, M. Benoit, P. J. Shore, D. Voigt, and J. VanDecar (2006). P and S velocity structure of the upper mantle beneath the Transantarctic Mountains, East Antarctic craton, and Ross Sea from travel time tomography, Geochem. Geophys. Geosys. 7, no. 7, doi: 10.1029/2005GC001238.
- Wessel, P., J. Luis, L. Uieda, R. Scharroo, F. Wobbe, W. H. Smith, and D. Tian (2019). The Generic Mapping Tools, version 6, *Geochem. Geophys. Geosys.* 20, no. 11, 5556–5564.
- Wiens, D. A., S. Anandakrishnan, J. P. Winberry, and M. A. King (2008). Simultaneous teleseismic and geodetic observations of the stick-slip motion of an Antarctic ice stream, *Nature* 453, no. 7196, 770–774.
- Wiens, D. A., R. C. Aster, A. A. Nyblade, P. D. Bromirski, P. Gerstoft, and R. A. Stephen (2024). Ross Ice Shelf displacement and elastic plate waves induced by Whillans Ice Stream slip events, *Geophys. Res. Lett.* 51, no. 7, doi: 10.1029/2023GL108040.
- Wiens, D. A., W. Shen, and A. J. Lloyd (2023). The seismic structure of the Antarctic upper mantle, in *The Geochemistry and Geophysics of the Antarctic Mantle*, A. P. Martin and W. van der Wal(Editors), Geological Society, London, Memoirs, London.
- Wilch, T., W. McIntosh, and K. Panter (2021). A Marie Byrd Land and Ellsworth Land: Volcanology, Geological Society, London, Memoirs, London.
- Wilding, J. D., W. Zhu, Z. E. Ross, and J. M. Jackson (2023). The magmatic web beneath Hawai, *Science* **379**, no. 6631, 462–468.
- Wimez, M., and W. Frank (2022). A recursive matched-filter to systematically explore volcanic long-period earthquake swarms, *Geophys. J. Int.* **231**, no. 2, 912–920.
- Winberry, J. P., and S. Anandakrishnan (2003). Seismicity and neotectonics of West Antarctica, *Geophys. Res. Lett.* **30**, no. 18, doi: 10.1029/2003GL018001.
- Winberry, J. P., S. Anandakrishnan, and R. B. Alley (2009). Seismic observations of transient subglacial water-flow beneath MacAyeal Ice Stream, West Antarctica, *Geophys. Res. Lett.* 36, no. 11, doi: 10.1029/2009GL037730.

- Winberry, J. P., A. D. Huerta, S. Anandakrishnan, R. Aster, A. Nyblade, and D. A. Wiens (2020). Glacial earthquakes and precursory seismicity associated with Thwaites Glacier calving, *Geophys. Res. Lett.* 47, doi: 10.1029/2019GL086178.
- Winter, K., D. Lombardi, A. Diaz-Moreno, and R. Bainbridge (2021). Monitoring icequakes in East Antarctica with the Raspberry Shake, Seismol. Res. Lett. 92, no. 5, 2736–2747.
- Withers, M., R. Aster, C. Young, J. Beiriger, M. Harris, S. Moore, and J. Trujillo (1998). A comparison of select trigger algorithms for automated global seismic phase and event detection, *Bull. Seismol. Soc. Am.* 88, no. 1, 95–106.
- Woollam, J., J. Münchmeyer, F. Tilmann, A. Rietbrock, D. Lange, T. Bornstein, T. Diehl, C. Giunchi, F. Haslinger, D. Jozinović, et al. (2022). Seisbench–A toolbox for machine learning in seismology, Seismol. Res. Lett. 93, no. 3, 1695–1709.
- Woollam, J., A. Rietbrock, A. Bueno, and S. De Angelis (2019). Convolutional neural network for seismic phase classification, performance demonstration over a local seismic network, *Seismol. Res. Lett.* **90**, no. 2A, 491–502.
- Yoon, C. E., E. S. Cochran, E. A. Vanacore, V. Huerfano, G. Báez-Sánchez, J. D. Wilding, and J. Smith (2023). A detailed view of the 2020–2023 southwestern Puerto Rico seismic sequence with deep learning, *Bull Seismol Soc Am.* doi: 10.1785/0120220229.
- Zandomeneghi, D., P. Kyle, P. Miller, C. M. Snelson, and R. Aster (2010). Seismic tomography of Erebus volcano, Antarctica, *Eos Trans. AGU* **91**, no. 6, 53–55.
- Zhang, M., W. L. Ellsworth, and G. C. Beroza (2019). Rapid earth-quake association and location, *Seismol. Res. Lett.* **90**, no. 6, 2276–2284.
- Zhu, W., and G. C. Beroza (2019). Phasenet: A deep-neural-network-based seismic arrival-time picking method, *Geophys. J. Int.* **216**, no. 1, 261–273.
- Zoet, L. K., S. Anandakrishnan, R. B. Alley, A. A. Nyblade, and D. A. Wiens (2012). Motion of an Antarctic glacier by repeated tidally modulated earthquakes, *Nature Geosci.* 5, no. 9, 623–626.

Manuscript received 27 February 2024 Published online 31 July 2024